water

MDPI

Article

Eco-Compensation Schemes for Controlling Agricultural Non-Point Source Pollution in Maoli Lake Watershed

Yumei Zheng [1,2], Guangchun Lei [1,*] and Peng Yu [3]

[1] School of Ecology and Nature Conservation, Beijing Forestry University, Beijing 100083, China; bubuer@163.com
[2] Business School, Central South University of Forestry and Technology, Changsha 410004, China
[3] Academy of Engineering Innovation, China Construction Fifth Engineering Division Corporation Limited, Changsha 410004, China; yupeng2017@foxmail.com
* Correspondence: guangchun.lei@foxmail.com

Abstract: Maoli Lake is the water source for local residents and a national nature protected area. However, due to intensive agriculture development, the water quality has deteriorated over the past decades. An effective measure to improve water quality is to control the agricultural non-point source (NPS) pollution through elaborate schemes based on eco-compensation. In order to develop such eco-compensation schemes, three scenarios of agricultural activity adjustment were designed: S1 (halving fertilization every year), S2 (fallow every other year), and S3 (returning agricultural land to forest). A Soil and Water Assessment Tool (SWAT) model was adopted to simulate runoff, total nitrogen, and total phosphorus. Based on SWAT results, a multi-criteria spatial evaluation model considering the environmental, economic, and social effects of eco-compensation was created for best scenario decision. The results reveal the following: (1) the total nutrients loss of agricultural land reduces in all scenarios, but S2 has more reduction compared to S1 and S3; (2) from the comprehensive perspective of environment–economy–society effects, S2 is the best scenario for rice land and dry land; (3) the comprehensive effect of eco-compensation at the grid scale has a significant spatial difference, and therefore, we highlight the necessity and significance of controlling agricultural NPS pollution by eco-compensation on a precise spatial scale. This study can broaden the application field of the SWAT model and provide a scientific basis and experience for the evaluation and spatial design of agriculture eco-compensation.

Keywords: eco-compensation; SWAT; non-point pollution; lake watershed; scenarios simulation; multi-criteria spatial evaluation

Citation: Zheng, Y.; Lei, G.; Yu, P. Eco-Compensation Schemes for Controlling Agricultural Non-Point Source Pollution in Maoli Lake Watershed. *Water* **2021**, *13*, 1536. https://doi.org/10.3390/w13111536

Academic Editor: Richard Cooper

Received: 22 April 2021
Accepted: 24 May 2021
Published: 30 May 2021

Publisher's Note: MDPI stays neutral with regard to jurisdictional claims in published maps and institutional affiliations.

Copyright: © 2021 by the authors. Licensee MDPI, Basel, Switzerland. This article is an open access article distributed under the terms and conditions of the Creative Commons Attribution (CC BY) license (http://creativecommons.org/licenses/by/4.0/).

1. Introduction

According to data published by the United States Environmental Protection Agency in 2000, approximately 30–50% of surface water in the world was affected by non-point source (NPS) pollution at the end of the last century. The NPS pollution caused by agricultural activities has gradually become the main cause of regional water environment deterioration [1,2]. The composition and the mechanism of agricultural NPS pollution are complex; its types are diverse, and its migration path is not clear. Moreover, water pollution has many influence factors, such as space, time, climate, soil topography, hydrology, and management measures [3–5]. At present, the comprehensive and quantitative description on the complex NPS pollution process in the whole watershed has been being considered as one of the best ways to quantitatively estimate NPS pollution, analyze the influence factors of pollution, and evaluate the effects of pollution control measures [6–8].

The NPS pollution models [9] mainly include two categories: empirical model and mechanism model. The representative empirical models include the soil conservation service (SCS) model [10], universal soil loss equation (USLE) model [11], and output coefficient model [12]. These models mainly use pollutant output coefficients to estimate the NPS pollution load output and are mostly used to evaluate the relationship between land use and lake eutrophication [13]. The mechanism model considers the internal mechanism of NPS pollution occurrence, migration, transformation, and environmental impact [14]. The CREAMS (chemicals, runoff, and erosion from agricultural management systems) model [15], the ANSWERS (areal non-point source watershed environment response simulation) model [16], the HSPF (hydrological simulation Program–Fortran) model [17], and the SWAT (Soil and Water Assessment Tool) model [18] have been widely used. Among these, the SWAT model [19], developed by the Agricultural Research Institute of the United States Department of Agriculture in the early 1990s, can simulate the effects of climate change, land use change, and agricultural management measures on the water cycle, sediment, nutrients, and crops. As a typical distributed hydrological model, it is widely used for long-term prediction and to simulate NPS pollution at the watershed scale [20–22].

Implementing best management practices (BMPs) at the watershed scale is one of the most effective measures for controlling NPS pollution [23,24]. The eco-compensation approach [25] in BMPs has a wide range of utility and can appropriately address problems of dispersion, randomness, scale, hysteresis, and difficulty of monitoring NPS pollution [26], which make it an efficient measure for control agricultural NPS pollution [27]. "Eco-compensation" is an institutional arrangement that focuses on the protection and sustainable utilization of ecosystem services and mainly adjusts the interest relationship of stakeholders through economic means [28], and in this paper, it refers to a series of approaches composed of "adjustment measures on agricultural land use" and "economic compensation to stakeholders". Since the second half of the last century, eco-compensation, also known as the payment for environment and ecosystem services, has gradually become an important policy tool to deal with the contradiction between the development of human society and the resource environment [29,30]. Agricultural land is a semi-natural ecosystem and a major subsystem in the agricultural ecosystem. It is not only restricted by the laws of nature but also affected by the social and economic activities of humans [31]. Agricultural eco-compensation can externalize the value of agricultural land ecosystem services by compensating the providers of the ecological value of agricultural land [32]. Eco-compensation measures for farmers have been widely implemented in the practice of protecting and restoring agricultural land ecosystems and reducing the environmental impact of agricultural land use [33–36]. The current research of eco-compensation on preventing and controlling agricultural NPS pollution mainly includes the evaluation of household willingness to improve the water environment quality by eco-compensation [37,38], the decision-making of a compensation plan in the best management practice of watershed agricultural land [39], and the comparative analysis of "cost–benefit" of eco-compensation [40]. There were also some interdisciplinary studies based on SWAT, such as scenario assessment of environmental impact of ecological engineering [41], impact of climate change on ecosystem habitats [42], and impacts of land-use conversion on the water cycle [43]. However, there are very few studies with comprehensive consideration of the impacts of eco-compensation scenarios on nutrient response, regional society, and economy. There is even less research on the spatial evaluation of eco-compensation scenarios.

Maoli Lake is the reservoir lake in Hunan Province, China. It is also a drinking water source for tens of thousands of residents and a site of a national wetland park. The agriculture in the Maori Lake Watershed is mainly family-scale traditional farming, including rice, vegetables, cotton, etc. Since the 1990s, due to the continuous high-intensity and intensive development of agriculture in this region, the eutrophication of lakes and streams continued to intensify, and the water quality of Maoli Lake declined to Class V around

2013 [44]. According to the Chinese standard GB3838-2002 "Surface Water Environmental Quality Standard", the water quality is divided into five grades; the larger the number, the worse. Monitoring results in 2018 showed the water quality of MLW had not been fundamentally improved, and the problem of water eutrophication was still prominent. These problems have been seriously affecting the supply of ecosystem services in this region and the sustainable development of this watershed. The aims of this study include (1) assessing improvement of water quality within the MLW by simulating nutrient process under different agricultural eco-compensation scenarios with a verified SWAT model; (2) evaluating the comprehensive effect of the eco-compensation scenarios on precise grid scale and conducting the optimum scenarios selection.

2. Materials and Methods

2.1. Study Site

The Maoli Lake Watershed in Changde City, Hunan Province, China was selected as the research area (Figure 1). It belongs to the Dongting lake system and has a control area of 387.63 km² (111°51′–111°58′ E, 29°20′–29°29′ N). The watershed belongs to the humid monsoon climate zone at the transition from the middle subtropical zone to the north subtropical zone. Its average annual precipitation is 1164.3 mm, and the average annual temperature is 16.6 degrees Celsius. Since the 1990s, due to the sustained and high-intensity development of agriculture within this area, the nutrient levels of streams and lakes have been increasing, and the water quality has been classified as Class V [43]. Since 2011, the local government has implemented a series of measures for preventing and controlling NPS pollution in the watershed. However, the watershed usually has high rainfall, and the agricultural land area accounts for more than 70% of the total area. The main agricultural land types in the study area include rice land, dry land, orchard, forest, and grassland. The rice land is mainly used for interplanting rice with rapeseed, vegetables, and other crops. The dry land is mainly used for rapeseed, cotton, vegetables, wheat, and other crops.

2.2. SWAT Model

The SWAT model is a distributed hydrological model based on a physical mechanism, which was developed by the Agricultural Research Center of the United States Department of Agriculture in 1994 based on the Simulator for Water Resources in Rural Basin (SWRRB) model [19]. During later development processes, some modules in the CREAMS model, environmental policy-integrated climate (EPIC) model, and other similar models were integrated into the SWAT model. The SWAT model has been widely used to simulate hydrological process [45], sediment yield process [46], and transfer process of agricultural chemical pollutants load [47]. According to the formation and occurrence mechanism of NPS pollution, the SWAT model is mainly composed of a hydrological process simulation module, soil erosion module, and pollution load module [48]. According to the differences among land use types, soil types, and slopes in different regions, the watershed is divided into several sub-watersheds, and each sub-watershed is divided into several hydrological response units (HRUs).

The SWAT model separate hydrologic simulation into land phase and routing phase. The driving force in the land phase is the water balance equation:

$$SW_t = SW_0 + \sum_{i=1}^{t}\left(R_{day} - Q_{surface} - E_a - W_{seep} - Q_{gw}\right) \quad (1)$$

In Equation (1), SW_t represents final soil moisture content, (mm); SW_0 represents soil moisture of the previous day, (mm); t represents total time, (day); R_{day} represents the precipitation in the i-th day, (mm); $Q_{surface}$ represents the surface runoff in the i-th day, (mm); E_a represents the evapotranspiration in the i-th day, (mm); W_{seep} represents the amount of percolation and bypass flow exiting the soil profile bottom in the i-th day, (mm); Q_{gw} represents the recharge water in the i-th day, (mm).

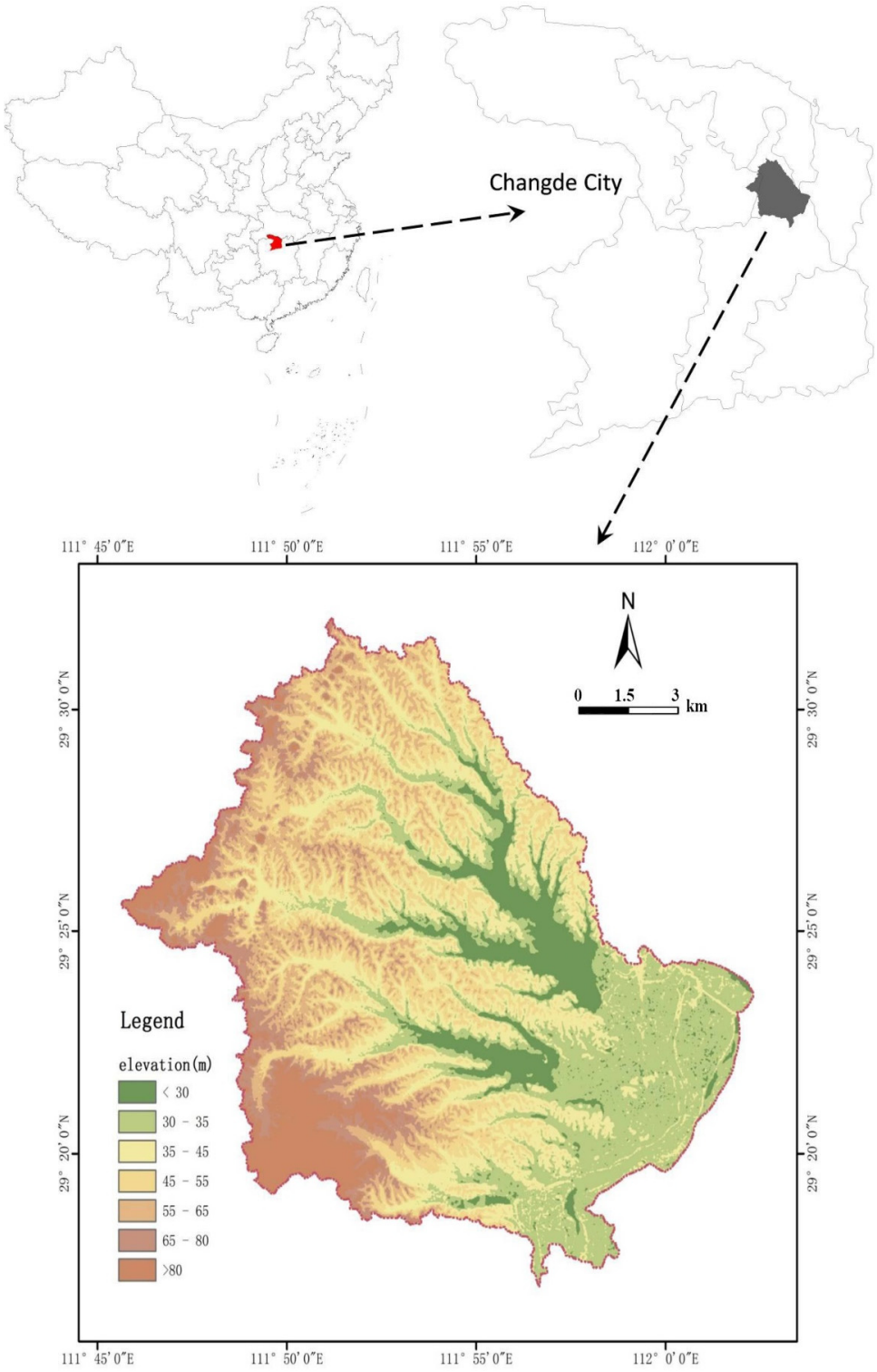

Figure 1. Research area description.

After finishing the calculation of the land phase, the water transport enters the routing phase, where sediments, nutrients, and other organic chemicals are transported via water. The SWAT model provides two routing models [48] for users: characteristic river length method and Muskingum method. The characteristic river length method was adopted in this research. The universal soil loss equation [49] is used to calculate erosion caused by rainfall and runoff in the SWAT model of this research:

$$SED = 11.8\left(Q_{surf} \cdot Q_{peak} \cdot AREA_{HRU}\right)^{0.56} \cdot K_{USLE} \cdot C_{USLE} \cdot P_{USLE} \cdot LS_{USLE} \cdot CFRG \quad (2)$$

In Equation (2), SED is the sediment yield in a given day, (tons); Q_{surf} is the surface runoff volume, (mm/ha); Q_{peak} is the peak runoff rate, (m^3/s); $AREA_{HRU}$ is the area of the HRU, (ha); K_{USLE} is the USLE soil erodibility factor, ($0.013 t \cdot m^2 \cdot hr/(m^3 \cdot t \cdot cm)$); C_{USLE} is the USLE cover and management factor; P_{USLE} is the USLE support practice factor; LS_{USLE} is the USLE topographic factor; $CFRG$ is the coarse fragment factor.

The entire nutrient cycling process of nitrogen and phosphorus can be simulated by the SWAT model. In this model, partial nitrogen is absorbed by the plant, and nitrate and organic nitrogen may be removed from the soil via water flow. The amount of nitrate nitrogen contained in runoff, lateral flow, and percolation is estimated by the product of water volume and the average concentration of nitrate in the layer. Organic nitrogen transported by sediment is calculated with an empirical loading function [50,51]. As for the phosphorus, the transport mechanism of organic phosphorus is similar to that of organic nitrogen. The amount of soluble phosphorus removed in runoff is predicted by the solution phosphorus concentration in the top 10 mm of soil, the runoff volume, and a partitioning factor [48,52].

2.3. Description of Input Data for SWAT

In order to construct the SWAT model, digital elevation model, soil, land use map, weather, measured runoff, and water quality data were utilized. For better water quality simulation, local agricultural management information was also required. These data are detailed in Table 1.

Table 1. Main input data of SWAT model of Maoli Lake Basin.

Data Description	Source	Resolution
Digital elevation model	Computer Network Information Center of Chinese Academy of Sciences: Geospatial Data Cloud Platform	30 m
Soil type	National Earth System Science Data Platform: Cold and Arid Regions Scientific Center	1 km
Land use map	Government sector	10 m
Weather data	National Centers for Environmental Prediction Climate Forecast System Reanalysis	Daily
Measured precipitation	Lixian Meteorological Bureau, Anxiang Meteorological Bureau in Hunan Province	Daily
Measured runoff[1]	Government data	Daily
Measured water quality[2]	Monitoring	Monthly
Agricultural management	Investigation	—

[1] The Doppler flowmeter and no-contact ultrasonic water gauge were used to measure velocity and water level of runoff; the common bottle sampler was used for sediment sampling, and the samples were treated by drying method.
[2] The water quality indicators are total nitrogen (TOT_N) and total phosphorus (TOT_P).

2.4. Parameters Sensitivity Analysis, Calibration, and Validation

In this research, the MLW was defined as 80 sub-watersheds and further divided into 2460 HRUs. The SWAT calibration and uncertainty program (SWAT-CUP) [53] was chosen to analyze the uncertainty and calibrate the parameters. The previous studies [21,53,54] have demonstrated its applicability. The sequential uncertainty fitting algorithm integrated in SWAT-CUP was used for parametric sensitivity and calibration. Owing to limited data, the calibration and validation periods of runoff were set as October

2014–April 2016 and May 2016–November 2017, respectively; the calibration and validation periods of nutrients were January 2014–December 2015 and January 2016–December 2017, respectively. The sampling site was located in Baiyian Creek, which is near the entrance of Maoli Lake (111°52′24.58″ E, 29°28′7.21″ N).

According to the relevant research [55–57] and fully considering the characteristics of MLW, 12 parameters for runoff and 11 parameters for nutrients with higher sensitivity were selected to analyze uncertainty and perform calibration (more details are shown in Appendix A).The Nash–Sutcliffe efficiency (NSE) coefficient, determination coefficient R^2, and relative volume error (RVE) were used to evaluate the performance of the SWAT model. According to Moriasi [58] and Mamo [59], for monthly runoff simulation, if NSE > 0.5, −10 < RVE < 10, and $R^2 > 0.6$, the simulation performance can be satisfactory; for monthly nutrient simulation, if NSE > 0.35, −10 < RVE < 10, and $R^2 > 0.3$, the simulation performance can be satisfactory.

Table 2 shows the simulated and observed monthly runoff, total nitrogen, and total phosphorus from October 2014 to November 2017. Although the NSE coefficient of the calibration period is only 0.619, the validation period is 0.712, which is close to the application requirement of 0.70. The RVE of calibration period is 4.22 and the validation period is −1.77, which indicates that the simulation deviation is relatively small and meets the application requirement. According to the research of Rahbeh [60], it is qualified for runoff simulation.

Table 2. Statistic of evaluation indices of the SWAT model. NSE: Nash–Sutcliffe efficiency; RVE: relative volume error.

Factor	Period	NSE	R^2	RVE
Runoff	Calibration period (October 2014–April 2016)	0.619	0.68	4.22
	Validation period (May 2016–November 2017)	0.712	0.71	−1.77
TOT_N[1]	Calibration period (January 2014–December 2015)	0.45	0.5	1.51
	Validation period (January 2016–December 2017)	0.25	0.45	1.92
TOT_P[1]	Calibration period (January 2014–December 2015)	0.48	0.58	6.50
	Validation period (January 2016–December 2017)	0.45	0.3	−0.98

[1] The number of measured data of TOT_N is 36, and so is TOT_P.

In line with Figure 2, it can be inferred the model produces an obvious error in the simulation of 2016 (wet year), which affects the fitting effect of the simulation results in the whole evaluation period to a certain extent. On the whole, the simulation effect is acceptable. The simulation results also can be seen in Figures 3 and 4. These values are qualified for nutrient simulation according to Rahbeh [54] excluding the validation period of TOT_N, which may be caused by the fact that the measured TOT_N and TOT_P data are not dense enough. Due to the limitation of the number of monitoring equipment and the distance between monitoring points, only one sample was used to calculate the concentration of TOT_N and TOT_P per month. This may be the main reason for such accuracy. However, the relative error between the simulated value and the measured value in each period is small, which indicates that the yearly simulations of TOT_N and TOT_P are accurate and can be used to evaluate the nutrient response on a planning scale.

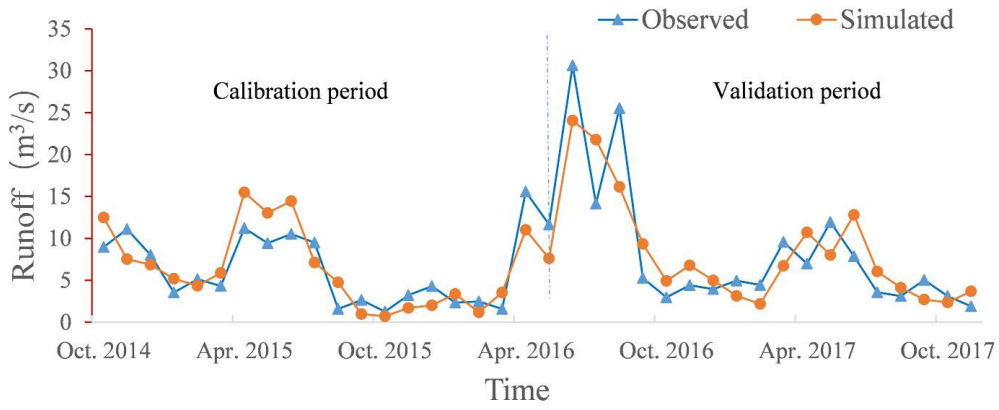

Figure 2. Comparision between simulated and observed runoff.

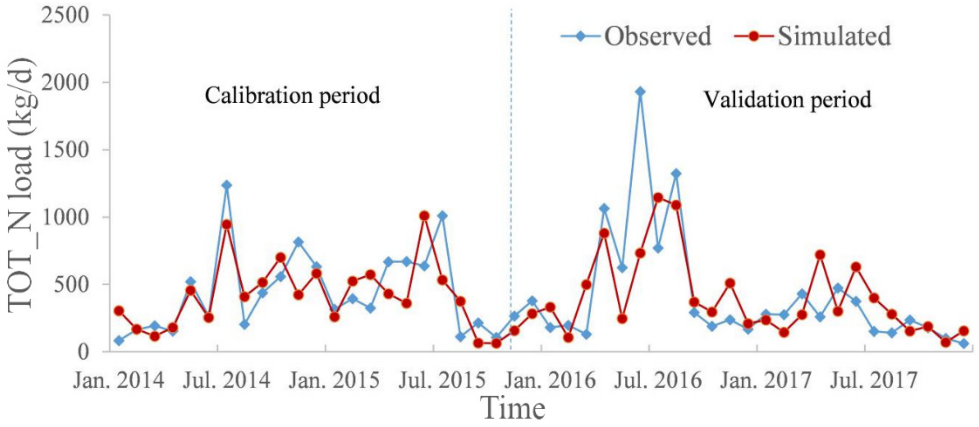

Figure 3. Comparison between simulated and observed result of TOT_N.

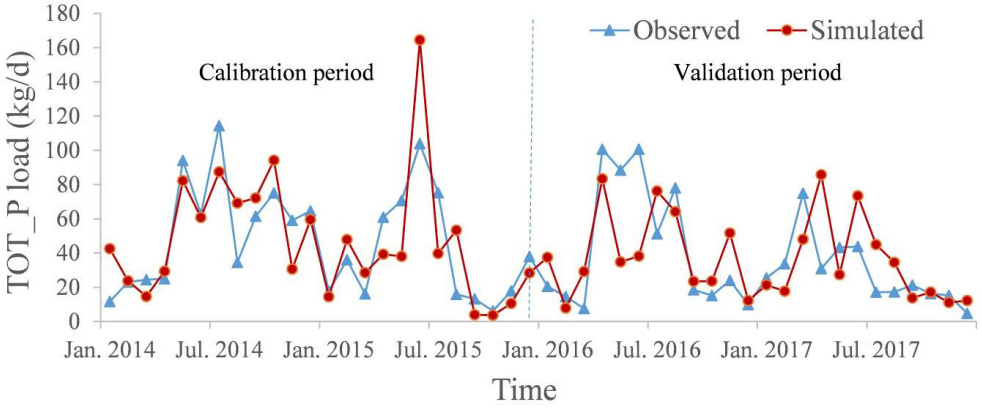

Figure 4. Comparison between simulated and observed result of TOT_P.

2.5. Scenarios Designs

Generally, the design of the eco-compensation scenario is based on the comprehensive consideration of multiple factors, such as the government policy background, the local social and natural status, and the investigation of stakeholders [61]. Since the beginning of the 20th century, China has successively implemented many ecological restoration projects closely related to eco-compensation [62], including the Grain for Green project,

fallow, and manure management. These measures have been implemented in many regions of China and achieved significant ecological and environmental benefits [63]. Based on the background of Chinese environmental policy, this research takes "nutrient input control" [64] as the key of mitigation of agricultural NPS pollution and designs 3 agricultural adjustment scenarios for the MLW. All scenarios are described in detail as follows, and the planting and fertilization management design of each scenario are displayed in Appendix B.

S0: Current situation. Under this scenario, the setting of fertilization and farming activities is maintained according to current practices.

S1: Halving fertilization every year. Under this scenario, the control of agricultural land fertilization in the watershed is emphasized. The amount of fertilizer applied to all rice land, dry land, and orchard is reduced in the whole watershed. This scenario is based on the assumption that farmers are fully publicized and reliably supervised by our village-level organization "village committee", which can guarantee that the fertiliser reduction measure can produce the expected results that is consistent with the SWAT calculated result.

S2: Fallow every other year. Under this scenario, the impact of fallow measures on the pollution load in the watershed is emphasized. This scenario was applied to all rice land and dry land in the watershed. Following normal farming in the first year, a grass-planting measure is implemented on agricultural land in the second year. Weeding is carried out at the end of the year, and the resulting biomass is kept as fertilizer. Normal farming resumes in the third year, and so on.

S3: Returning agricultural land to forest. Under this scenario, the impact of conversion measures on the pollution load in the watershed is emphasized. There are many lakes and rivers throughout the watershed, which may cause fertilizer to enter the watershed circulation to a greater extent. Thus, the condition for returning agricultural land to the forest is formulated: rice land and dry land within 200 m from the lake and 100 m from the main water system can be changed from agricultural land to forest.

2.6. Construction of Evaluation Model for Ecological Ccompensation Scenarios

The AHP combined with GIS, one of the most effective methods for multi-attribute ranking/weighting problem, has been widely used in the field of environmental policy evaluation and decision making [65]. In order to evaluate eco-compensation scenarios, a spatial multi-criteria evaluation (SMCE) model is constructed with the analytic hierarchy process (AHP) as the core component [66] in this paper.

2.6.1. Construction of Hierarchy Structure of Comprehensive Evaluation Model

The previous research studies show that the expression for the comprehensive effect of environment policy is usually based on a collaborative perspective of social, economic, and environmental dimensions [67]. Therefore, we build the SMCE to evaluate the comprehensive effect of eco-compensation scenarios from these three dimensions. The "nitrogen and phosphorus reduction" is choosen as the indicator of environmental effect [68]. The "farmland income" is choosen as the indicator of economic effect [69], and the "participation willingness of eco-compensation" is choosen as the indicator of social effect [36]. Taking spatial agricultural land grid as the basic computing unit [70], the comprehensive effect evaluation of farmland use based on these indicators can be carried out using the GIS platform. Figure 5 shows the framework and index system of the SMCE model.

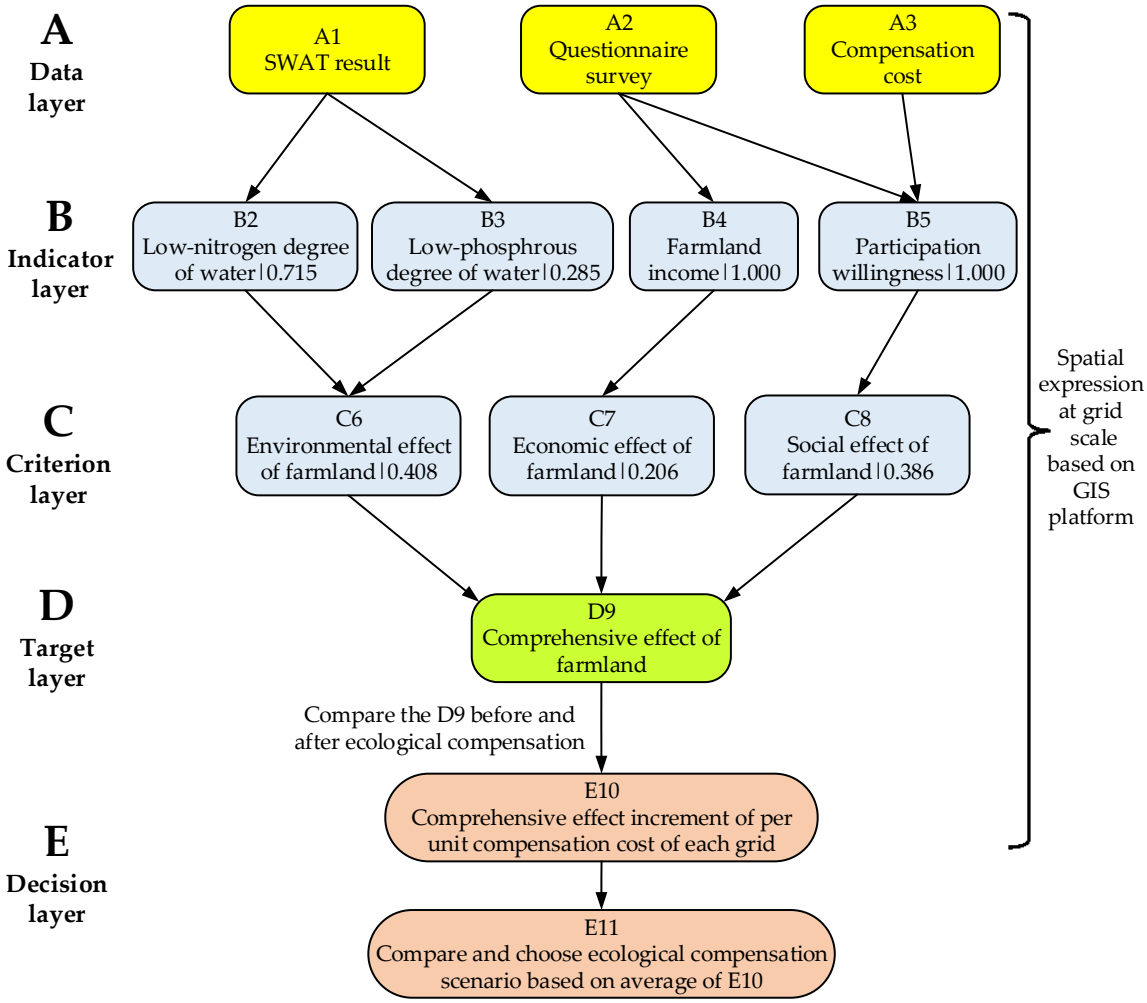

Figure 5. Hierarchy structure of comprehensive evaluation model (where the number after "|" is weight).

2.6.2. Determination of Data Layer

The 10-m square farmland grid is the basic unit of the model operation, and a total of 1,350,727 grids of agricultural land in MLW were divided by GIS software. Only two existing land use types, rice land and dry land, are calculated, because the area of orchards only accounts for 2.35% of the total watershed area, and its compensation measure is only in S1. The spatial distribution map of farmland and the S3 target region is shown in Figure 6.

The input data for the SMCD model were derived from SWAT simulation results of HRU scale, and the eco-compensation questionnaire survey involves 370 householders in MLW between 2018 and 2019. It is assumed that there is a total of j grids for eco-compensation, and the values of $B2$ (low-nitrogen degree of water) and $B3$ (low-phosphorus degree of water) of the grid can be obtained by normalizing the difference of the maximum value of all grids in the SWAT simulation results minus the value of this grid (Equations (3) and (4)). The input values of $B4$ (farmland income) and $B5$ (participation willingness) are obtained from the questionnaire survey, and different types of farmland are assigned different values.

$$B2_i^s = [\max(TOT\_N_k^s) - TOT\_N_i^s]/\max(TOT\_N_k^s);\ k = 1,2,3,\ldots,j;\ s \in \{S0, S1, S2, S3\} \quad (3)$$

$$B3_i^s = [\max(TOT\_P_k^s) - TOT\_P_i^s]/\max(TOT\_P_k^s);\ k = 1,2,3,\ldots,j;\ s \in \{S0, S1, S2, S3\} \quad (4)$$

The annual compensation (*COST*) in different scenarios and the corresponding input values of indicator layer *B* are shown in Table 3. The *COST* is determined according to the current policies launched by the local government in recent years and the relevant references [71,72].

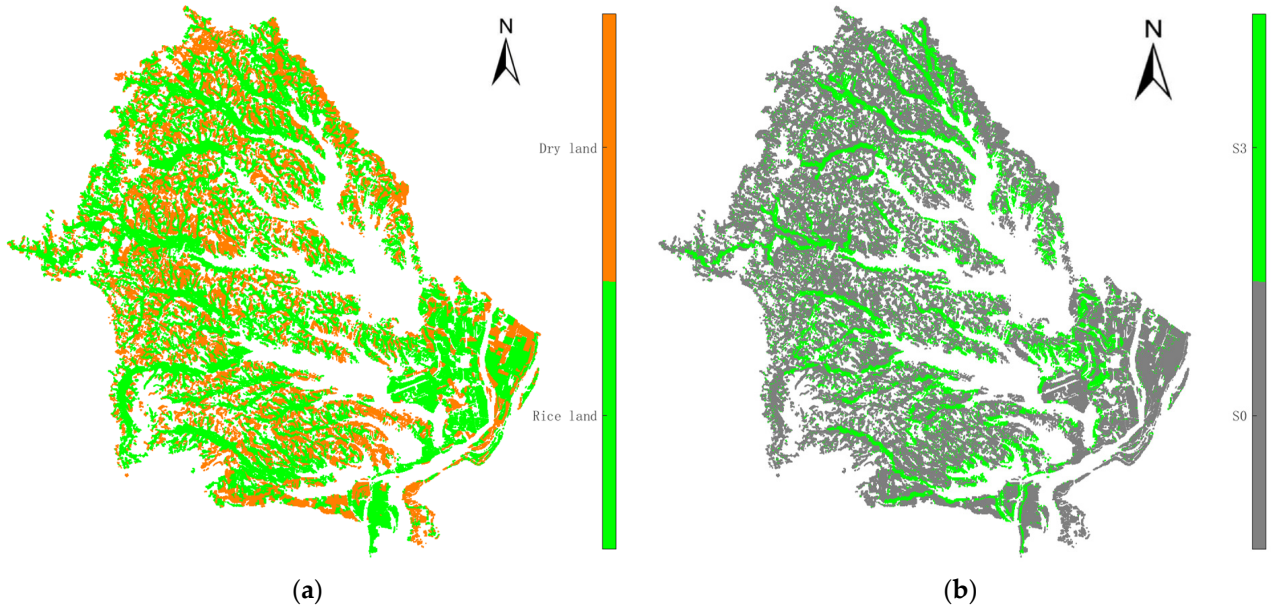

(**a**) (**b**)

Figure 6. The spatial distribution of farmland (**a**) and S3 target region (**b**) at grid scale.

Table 3. Input values of indicator layer of different types of land use in different scenarios. S0: current situation; S1: halving fertilization every year; S2: fallow every other year; S3: returning agricultural land to forest; B2: low-nitrogen degree of water; B3: low-phosphorus degree of water; B4: farmland income; B5: farmers' participation willingness.

Scenario	Farmland Type	COST[1]	B2	B3	B4	B5
S0	Rice land	0			1	0.667
S0	Dry land	0			0.905	0.667
S1	Rice land	715	The value of	The value of	0.857	0.786
S1	Dry land	715	each grid is	each grid is	0.81	0.813
S2	Rice land	525	calculated by	calculated by	0.762	0.895
S2	Dry land	525	Formula (2)	Formula (3)	0.667	1
S3	Rice land	500			0.345	0.482
S3	Dry land	500			0.345	0.478

[1] The unit of *COST* is yuan/(mu·yr), and the "mu" is a Chinese unit of land measurement that is commonly 666.7 square meters.

2.6.3. Determination of Weights

In order to determine the weight of indicators of each level, government staff, stakeholders, and experts in various fields are organized to conduct participatory discussion [73,74] where the AHP is used to score their opinions, and the average value of all their weights is used for the final weight value. The weight of AHP is determined by the way of stakeholder discussion, including government officials, stakeholders (farmers), and experts in various fields. The Balanced Scorecard method was used to collect and process data. The government officials came from the relevant departments that made the eco-compensation policy, including the local Ministry of Agriculture, the local Ministry of Environmental Protection, and the local Ministry of Finance. Each department appointed 1

representative. Farmers came from three town-level administrative regions in the study area, and each town appoints 1 person as its representative. The expert group included 1 expert each from agricultural environment science, economics, and sociology.

2.6.4. Model Decision

The SMCE model is used to calculate D9 (comprehensive effect of land use) of each grid, and the spatial differences of all grids can be analyzed. By comparing the changes of $D9$ before and after eco-compensation, $E10$ (the comprehensive effect increments of per unit compensation cost) of each grid can be calculated by Equation (5), and its spatial distribution can be mapped for decision-making analysis. Finally, the optimal eco-compensation scenario can be determined by comparing $E11$, which is the mean value of $E10$ of all grids (Equation (6)).

$$E10_i^s = [D9_i^s - D9_i^{S0}]/\mathrm{COST}_i^s \,; s \in \{S1, S2, S3\} \quad (5)$$

$$E11_i^s = 1/\mathrm{j} \cdot \sum_{i=1}^{j} E10_i^s \,; s \in \{S1, S2, S3\} \quad (6)$$

3. Results

3.1. Characteristics of NPS Pollution Load in MLW

3.1.1. Temporal Distribution

Based on the simulation results of S0, the basic characteristic of NPS pollution load in the study area can be analyzed. Figure 7 describes the NPS pollution load of TOT_N and TOT_P in the 8-year simulation period. The interannual difference of TOT_N and TOT_P is obvious. The TOT_N in the simulation period is (1377.50 ± 374.28) t each year, and the TOT_P is (200.95 ± 78.96) t each year. The highest NPS nitrogen pollution load is 1583.14 t in 2015, and the highest NPS phosphorus pollution load is 235.83 t in 2016. The lowest values of nitrogen and phosphorus pollution are respectively 1003.22 t and 121.99 t in 2011.

Figure 8 shows the nutrient output of the months with abundant precipitation (Mar. to Jun.) is greater than that of other months throughout the year, and the nutrient output of the months with the least rainfall (Dec. to Feb. of the next year) is the least. The NPS pollution load is mainly concentrated in the wet season from Mar. to Jun. In 2011–2018, the nitrogen pollution load from Mar. to Jun. accounts for 66.51–78.38% of the whole year, and the phosphorus pollution load accounts for 61.29–78.69% of the whole year. According to the time distribution characteristic of NPS nitrogen and phosphorus pollution load in the MLW, Mar. to Jun. is the key period for the reduction of pollution. In this period, the management measures of fertilizer application, such as reducing fertilizer application and fallow, can effectively reduce the impact of NPS pollution in theory.

3.1.2. Spatial Distribution

During the simulation period, the annual average of the TOT_N nutrient loss load in different sub-watersheds ranges from 0 to 77.69 t, and the annual average of TOT_P nutrient loss load in different sub-watersheds ranges from 0 to 10.2 t. The distribution of TOT_N and TOT_P nutrient loss exhibits a similar differentiation law. The high value of nutrients was mainly concentrated in the 73th, the 75th, and the 77th sub-watersheds in the southwest of MLW. The contribution of pollution in the southwest mountainous area and near the central and western lake entrance is greater than that in the eastern flat area.

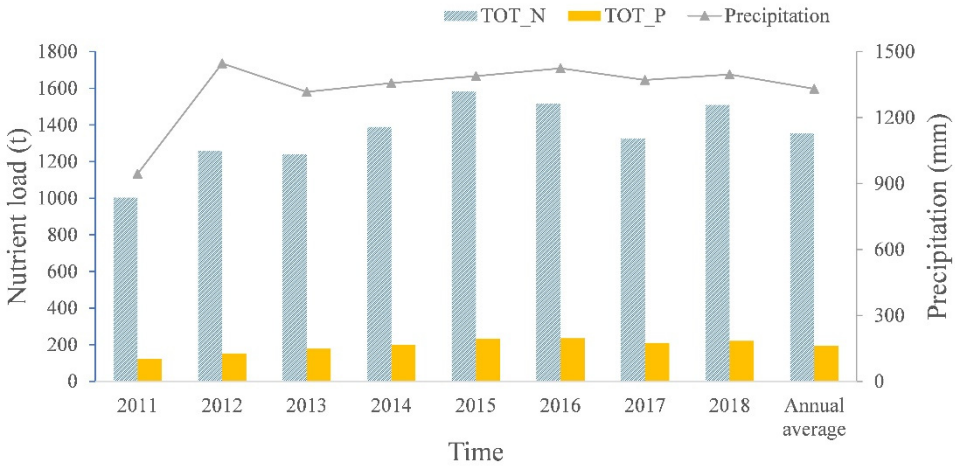

Figure 7. TOT_N and TOT_P of MLW from 2011 to 2018.

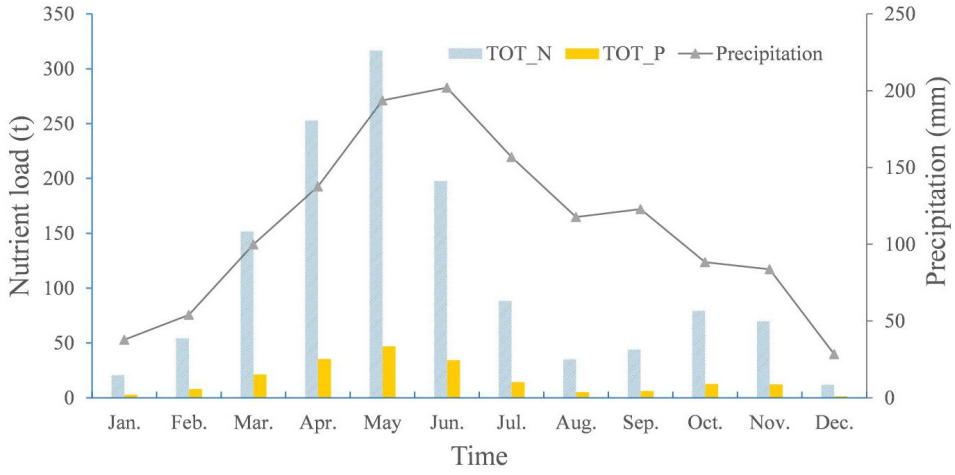

Figure 8. Average monthly nutrient load from 2011 to 2018.

3.2. Pollution Distribution under Eco-Compensation Scenarios

3.2.1. Temporal Distribution of Pollution under Eco-Compensation Scenarios

Figure 9 shows that the annual variation trend of nitrogen and phosphorus NPS pollution load is similar under each scenario. S1 is slightly better than S3 in decreasing the total amount of nitrogen and phosphorus, but its effect is not significant enough comparing to the fallow year of S2. S2 can reduce more nitrogen and phosphorus during the fallow year than other scenarios, but its nitrogen and phosphorus in the first year are nearly the same as S0. Except for the first year, the amount of nitrogen and phosphorus of S2 in subsequent farming years still has a certain reduction comparing to S1. This indicates that S2 can reduce nutrients not only in the fallow year but also in the farming year. Comprehensively considering the yearly scale, S2 works better than S1 and S3 in mitigating total nitrogen and phosphorus. Moreover, the monthly simulation results of TOT_N and TOT_P load (Appendix C) show that the decreased nutrient load of S2 is the largest comparing to the decrease of S1 and S3.

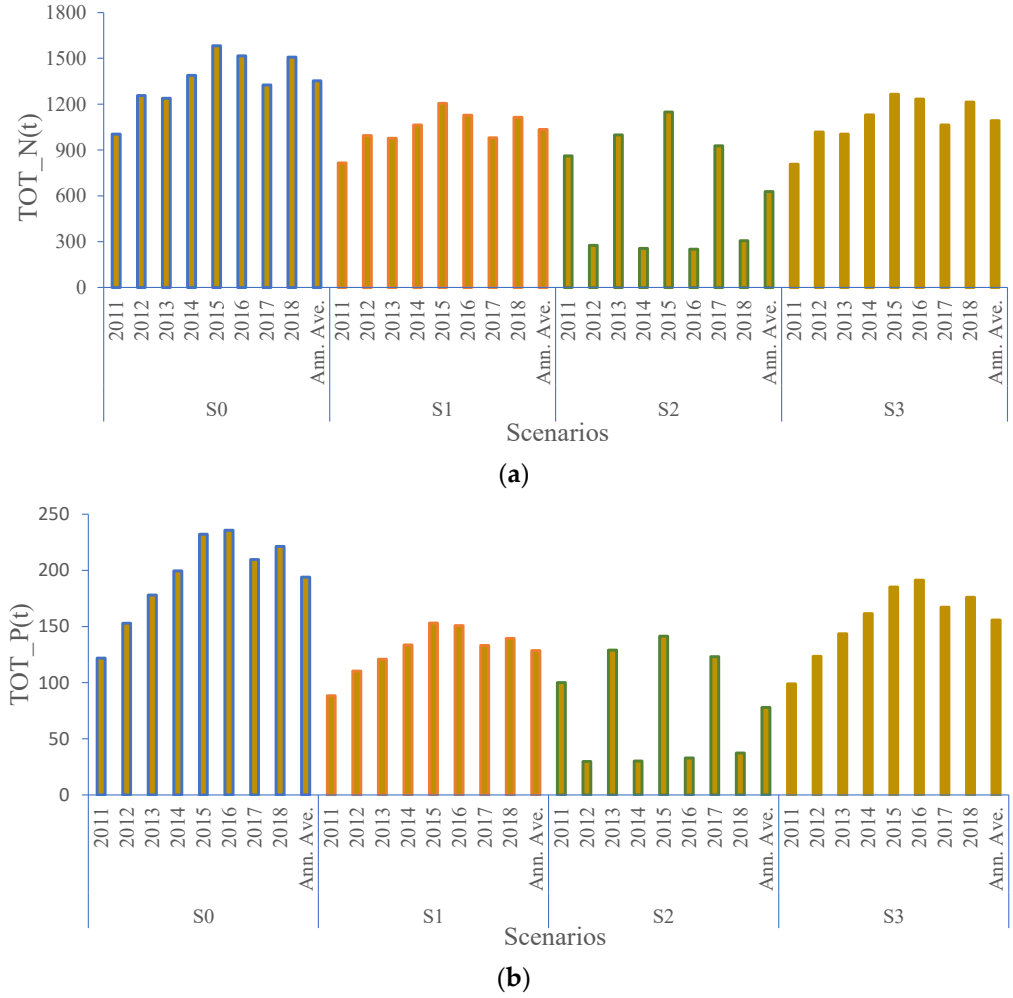

Figure 9. TOT_N (**a**) and TOT_P (**b**) pollution load of each scenario.

3.2.2. Spatial Distribution of Pollution Load under Eco-Compensation Scenarios

The spatial distribution of TOT_N and TOT_P in the S0 are shown in Figures 10 and 11. Figure 10 describes the distribution of annual NPS TOT_N load in the study area from 2011 to 2018 under each scenario. Taking 80 sub-watersheds as the control unit, the TOT_N load of each sub-watershed reduces in different degrees under different design scenarios compared to S0. The average annual loss load of TOT_N in the S1 is 0–62.21 t in different sub-watersheds; the average annual loss load of TOT_N in the S2 is 0–47.92 t, and that in the S3 is 0–77.69 t. Similar to S0, the high values of each scenario are mainly concentrated in the 57th, 59th, 62th, 63th, 76th, and 78th sub-watersheds, and the highest values are concentrated in the 73th, 75th, and 77th sub-watersheds in the southwest.

Figure 11 describes the average annual NPS TOT_P load distribution of each scenario from 2011 to 2018. The figure shows that the TOT_P load of each sub-watershed reduces in different degrees under different scenarios compared to S0. The average annual loss load of TOT_P in different sub-watersheds varied from 0 to 8.53 t under S1, from 0 to 7.34 t under S2, and from 0 to 10.2 t under S3. The spatial distribution of each scenario is similar to S0, and the high value of each scenario is mainly concentrated in the similar sub-watershed with S0.

3.2.3. Characteristic of NPS Pollution Load in Different Types of Agricultural Land

Table 4 shows the nutrient loss of different types of agricultural land in the study area under S0. When the HRU is used as the control unit, the average annual nitrogen loss of agricultural land (including rice land, dry land, orchard, forest, and grass land) was

1162.4 t, and phosphorus loss was 134.6 t. Rice land and dry land are the main types of agricultural land in the study area and main sources of nitrogen and phosphorus loss. The total area of rice land accounts for 28.87% of the watershed area, and its annual TOT_N loss is 672.1 t, which accounts for 57.82% of the total loss. The total area of dry land accounts for 16.53% of the watershed area, and its annual TOT_N loss is 436.25 t, which accounts for 37.53% of the total loss. The orchard accounts for 2.36% of the total agricultural land but contributes 3% of the total nitrogen loss. The forest land accounts for 19.68% of the total agricultural land but only contributs 0.8% of nitrogen loss and 1.41% of phosphorus loss. The percentages of contribution of grass land to nitrogen and phosphorus loss are 0.11% and 0.8%, respectively.

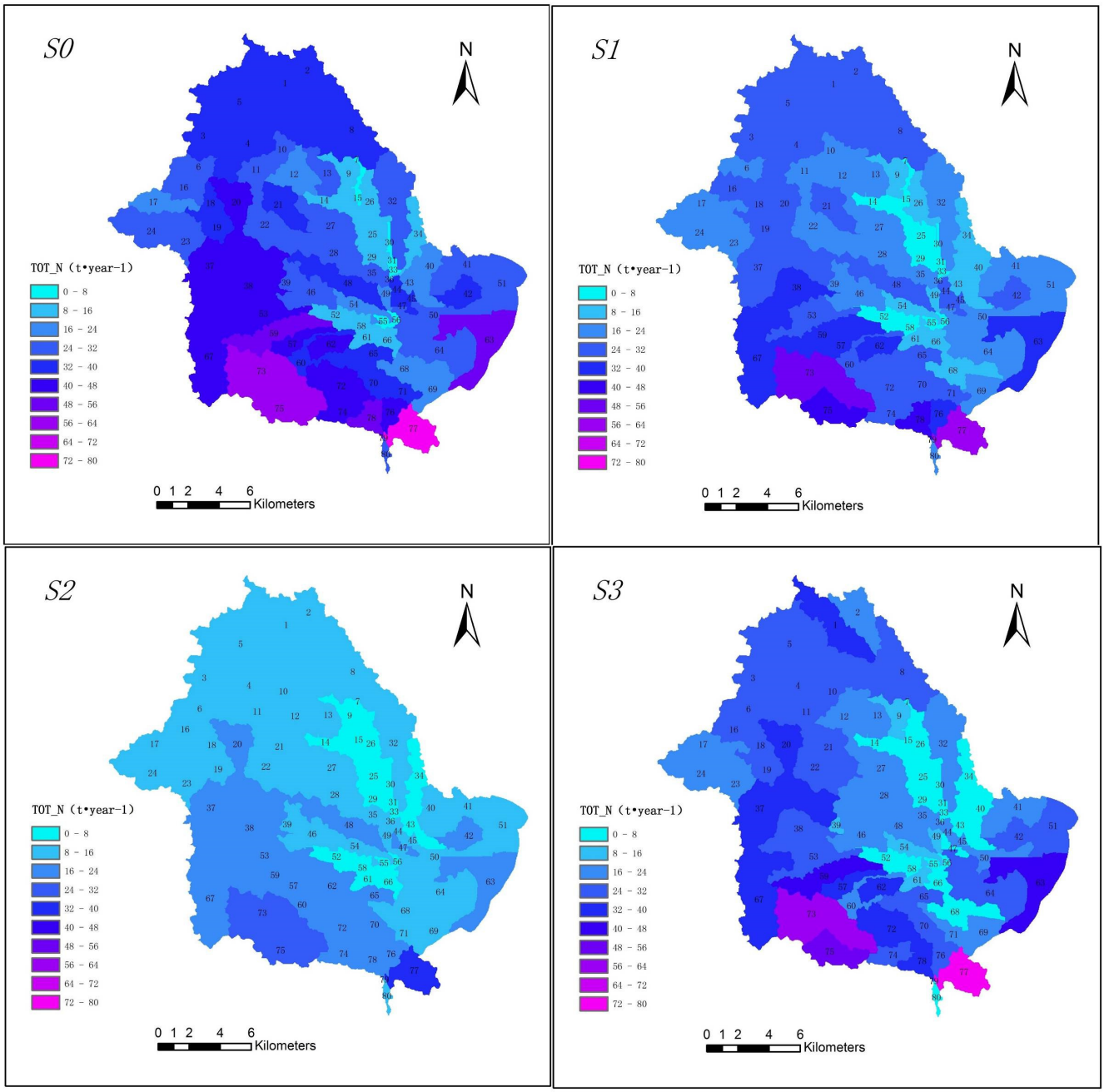

Figure 10. Spatial distribution of TOT_N loss in MLW under different scenarios. S0: current situation; S1: halving fertilization every year; S2: fallow every other year; S3: returning agricultural land to forest.

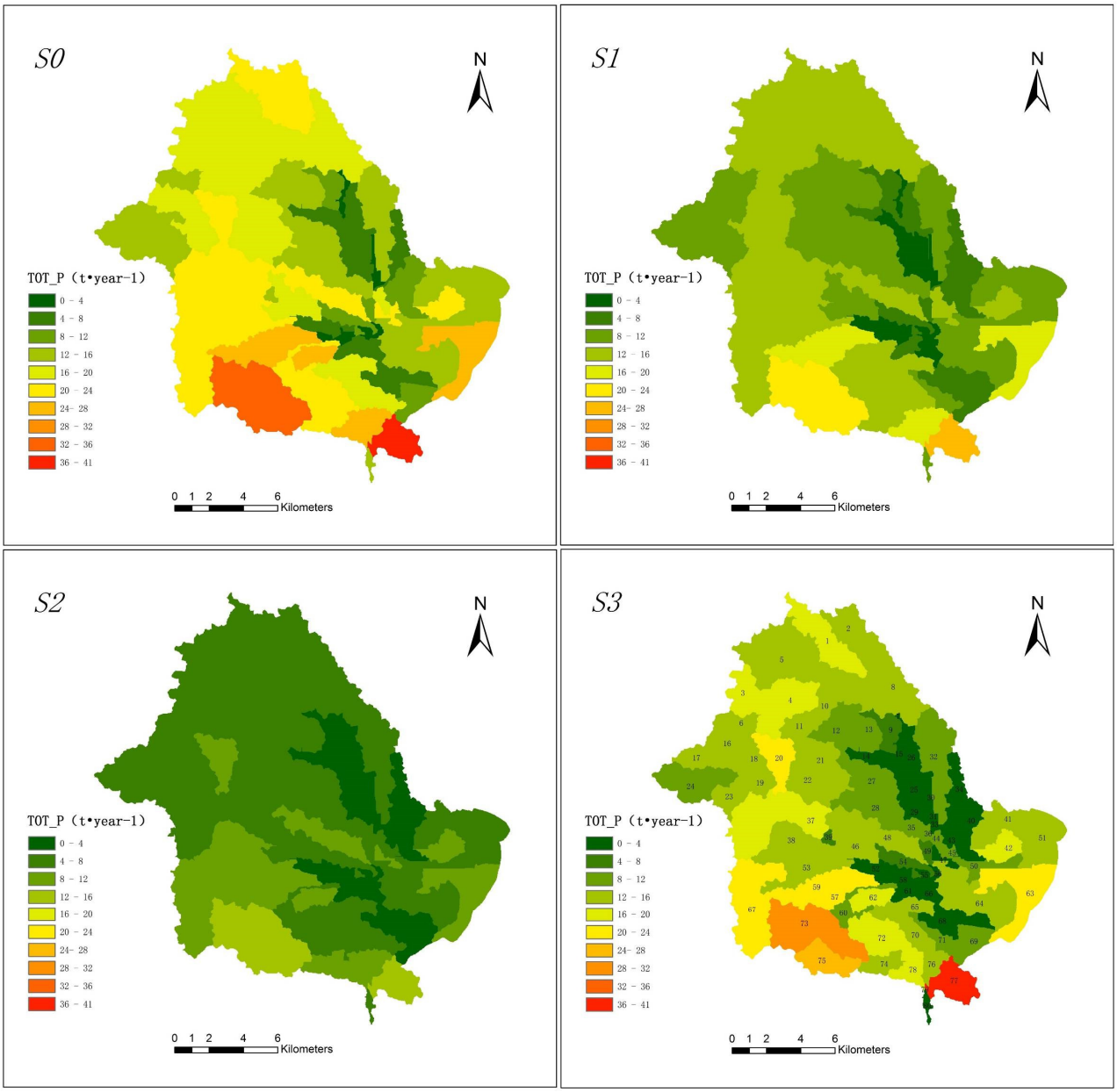

Figure 11. Spatial distribution of TOT_P loss in MLW under different scenarios. S0: current situation; S1: halving fertilization every year; S2: fallow every other year; S3: returning agricultural land to forest.

Table 4. Nutrient loss of different types of farmland in MLW.

Land Type	Data	Area/km²	TN/t	Organic N/t	Nitrate N/t	TP/t	Organic P/t	Inorganic P/t
Rice land	Value	112.00	672.10	99.70	572.40	63.81	7.24	56.57
	Percentage	28.87%	57.82%	42.28%	61.78%	47.41%	43.43%	47.97%
Dry land	Value	64.15	436.25	122.50	313.75	65.25	7.77	57.49
	Percentage	16.53%	37.53%	51.95%	33.86%	48.48%	46.57%	48.75%
Orchard	Value	9.15	34.87	0.11	34.76	0.48	0.01	0.48
	Percentage	2.36%	3.00%	0.05%	3.76%	0.36%	0.03%	0.41%
Forest	Value	76.35	9.30	5.59	3.71	1.90	0.68	1.22
	Percentage	19.68%	0.80%	2.36%	0.40%	1.41%	4.05%	1.03%
Grass land	Value	5.28	1.28	1.06	0.21	0.36	0.14	0.23
	Percentage	1.36%	0.11%	0.46%	0.02%	0.27%	0.80%	0.19%

Taking the agricultural land per unit area as the control unit, the comparison of TOT_N and TOT_P NPS load of different types of agricultural land in each scenario is illustrated in Table 5. Taking rice land as an example, under S0, the nitrogen loss rate reaches 62.33%, and the phosphorus loss rate is 11.06%. Under S1, the nitrogen use in rice land reduces by half, and the nitrogen loss rate reduces to 59.21%, which was 150.85kg·a^{-1} per hectare; the total nitrogen loss reduces by 52.51%, and the nitrogen loss rate reduces by 5.01%. Under S1, the use of phosphorus fertilizer in rice land also reduces by half, and the non-point phosphorus load reduces to 20.11 kg·a^{-1} per hectare. Compared with S0, the non-point phosphorus load reduces by 34.23%, but the phosphorus loss rate increases by 31.54%. The average annual nitrogen and phosphorus input, which is half of S0, in S2 is consistent with that in S1, but S2 exhibits better NPS pollution reduction efficiency than S1; in S2, the nitrogen loss rate reduces to 47.14%, and the phosphorus loss rate reduces to 7.62%. The values of total amount of nitrogen and phosphorus are respectively 120.11 kg·a^{-1} and 10.53 kg·a^{-1} per hectare and reduce by 62.18% and 65.57% comparing to S0, while the loss rates of nitrogen and phosphorus respectively reduce by 24.37% and 31.13% comparing to S0. However, under S3, the loss of nitrogen and phosphorus nutrients per unit area of rice land increased slightly, which were 328.23 kg·a^{-1} and 32.41 kg·a^{-1} per hectare, respectively. Compared with S0, the loss rates of nitrogen and phosphorus increase by 3.34% and 6.06%, respectively.

In each scenario as shown in Table 5, the load of the orchard is medium; the load of rice land and dry land is relatively high, and the load of forest and grass land is relatively low. The order of annual average loss load of nitrogen and phosphorus of agricultural land per unit area is: dry land > rice land > orchard > grass land > forest.

Table 5. Nutrient input and loss per unit area in different scenarios. S0: current situation; S1: halving fertilization every year; S2: fallow every other year; S3: returning agricultural land to forest.

Scenario	Land Type	Nitrogen Input (kg/ha)	Phosphate Input (kg/ha)	Nitrogen Load (kg/ha)	Phosphate Load (kg/ha)	Nitrogen Loss Rate (%)	Phosphate Loss Rate (%)	Change rate (%)			
								Nitrogen	Phosphate	Nitrogen Loss Rate	Phosphate Loss Rate
S0	Rice land	509.57	276.37	317.61	30.58	62.33	11.06	/	/	/	/
	Dry land	700.34	305.54	315.03	47.77	44.98	15.64	/	/	/	/
	Orchard	293.18	203.60	196.57	2.79	67.05	1.37	/	/	/	/
	Forest	0	0	7.13	1.48	/	/	/	/	/	/
	Grass land	0	0	13.56	3.75	/	/	/	/	/	/
S1	Rice land	254.79	138.19	150.85	20.11	59.21	14.55	−52.51	−34.23	−5.01	31.54
	Dry land	350.17	152.77	139.27	30.63	39.77	20.05	−55.79	−35.89	−11.58	28.21
	Orchard	146.59	101.80	99.42	1.19	67.82	1.17	−49.43	−57.32	1.15	−14.65
	Forest	0	0	7.13	1.48	/	/	0	0	/	/
	Grass land	0	0	13.56	3.75	/	/	0	0	/	/
S2	Rice land	254.79	138.19	120.11	10.53	47.14	7.62	−62.18	−65.57	−24.37	−31.13
	Dry land	350.17	152.77	110.09	17.22	31.44	11.27	−65.05	−63.96	−30.11	−27.92
	Orchard	293.18	203.60	196.57	2.79	67.05	1.37	0	0	0	0
	Forest	0	0	7.13	1.48	/	/	0	0	/	/
	Grass land	0	0	13.56	3.75	/	/	0	0	/	/
S3	Rice land	509.57	276.37	328.23	32.41	64.41	11.73	3.34	5.98	3.34	6.06
	Dry land	700.34	305.54	324.03	49.14	46.27	16.08	2.86	2.87	2.87	2.81
	Orchard	293.18	203.60	210.41	2.42	71.77	1.19	7.04	−13.26	7.04	−13.14
	Forest	0	0	6.10	1.11	/	/	−14.45	−25.00	/	/
	Grass land	0	0	13.46	3.72	/	/	−0.74	−0.80	/	/

The loads of nitrogen and phosphorus of rice land and dry land in S0 are the same as those in S3; the nitrogen load of the two types of land are similar, while the phosphorus load of dry land is slightly higher than that of rice land. In S1, the nitrogen and phosphorus load of rice land, dry land, and orchard significantly reduce, and the load difference among these three types of agricultural land reduces to a certain extent. The total NPS

load of S2 is lower than that of S1 because the loads of rice land and dry land in S2 are slightly lower than that of S1, and the load of the orchard is higher than that of rice land and dry land and becomes the highest load. Generally, rice land, dry land, and orchard are the main land of NPS pollution in the MLW. However, the NPS pollution in different areas of the watershed has different characteristics. Therefore, it is necessary to consider the probability of load loss of different nutrient in farmland when carrying out accurate prevention and control of NPS pollution load.

3.3. Results of SMCE Model and Evaluation of Eco-Compensation Scenarios

The SMCE model was used to evaluate the comprehensive effect of farmland utilization under different eco-compensation scenarios. The evaluation was carried out in each target farmland grid within the watershed, and corresponding quantitative values were obtained. In scenario S0/S1/S2, the grid counts of rice land and dry land were 839,207 and 511,520, respectively. In scenario S3, the grid count of rice land and dryl and were 199,223 and 89,215, respectively.

3.3.1. Spatial Distribution of D9 and E10 under Different Scenarios

The spatial distribution of D9 and E10 under each eco-compensation scenario is plotted as shown in Figures 12 and 13. It can be seen from the figures that the distribution of D9 and E10 in different scenarios is greatly different, and the significant spatial distribution difference also appears on the grid scale under a same scenario. As shown in Figure 13, based on the perspective of the whole watershed, the order of increment of comprehensive effect per unit compensation cost is S2 > S1 > S3.

3.3.2. Calculation Results of Indicators of Each Layer of SMCE Model

Table 6 shows the averages of all target grids of nodes of the SMCE model under different scenarios. By comparing C6, the order of environmental effects of eco-compensation scenarios is S3 > S2 > S1. By comparing C7, the economic effect of eco-compensation scenarios is S1 > S2 > S3. By comparing C8, it can be seen that the social effect of eco-compensation scenarios is S2 > S1> S3.

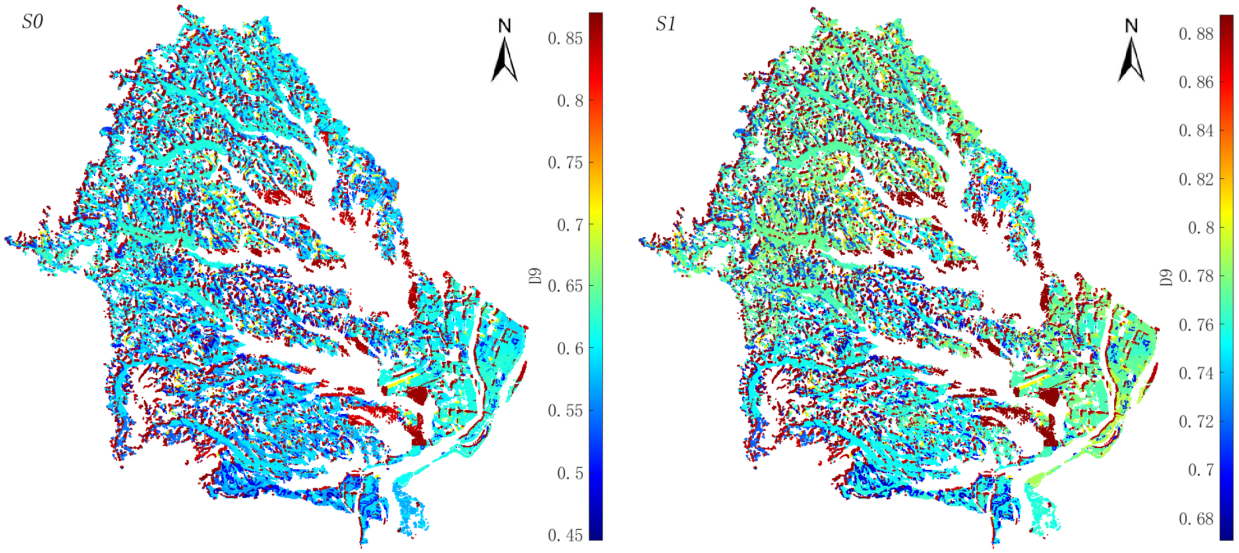

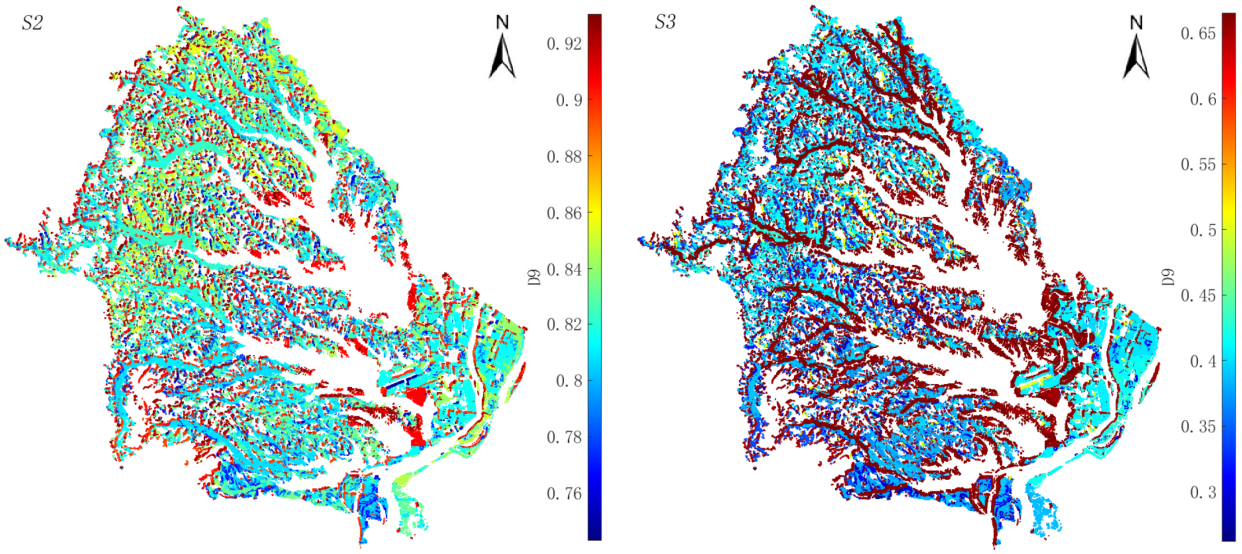

Figure 12. Spatial distribution of D9 under different scenarios. S1: halving fertilization every year; S2: fallow every other year; S3: returning agricultural land to forest.

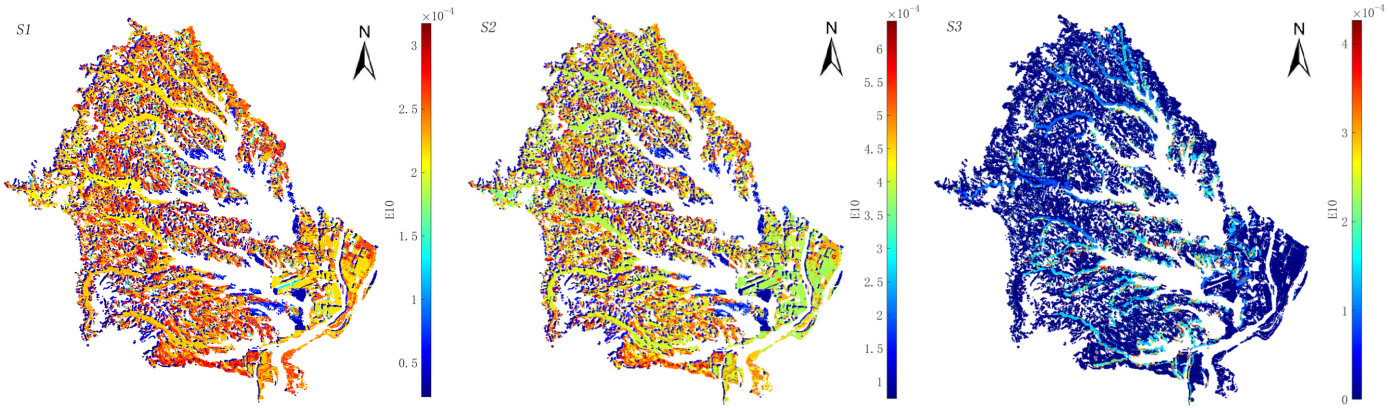

Figure 13. Spatial distribution of E10 under different scenarios. S1: halving fertilization every year; S2: fallow every other year; S3: returning agricultural land to forest.

Through the analysis of the results of D9 in Table 6, the comprehensive effects of all eco-compensation scenarios are improved to a different extent compared to those of S0. By comparing E10, it can be found that the E10 value of dry land is greater than that of rice land under each eco-compensation scenario. By combining the scenario with land type, it can be found that the E10 value in "S2 on dry land" is the highest, followed by "S2 on rice land", and the low E10 values appears in "S1 on rice land" and "S3 on rice land".

Table 6. Averages of all target grids of nodes of the SMCE model. B2: low-nitrogen degree of water; B3: low-phosphorus degree of water; C6: environmental effect of farmland; C7: economic effect of farmland; C8: social effect of farmland; D9: comprehensive effect of farmland; E10: comprehensive effect increment of per unit compensation cost of each grid; S0: current situation; S1: halving fertilization every year; S2: fallow every other year; S3: returning agricultural land to forest.

Scenario	Farmland Type	Averages of All Target Grids						
		B2	B3	C6	C7	C8	D9	E10
S0	Rice land	0.3735	0.7549	0.4822	1.0000	0.6670	0.6602	-
S0	Dry land	0.3796	0.6970	0.4701	0.9048	0.6670	0.6356	-
S1	Rice land	0.7144	0.8396	0.7501	0.8571	0.7860	0.7860	1.760×10^{-4}
S1	Dry land	0.7257	0.8040	0.7480	0.8095	0.8130	0.7858	2.100×10^{-4}
S2	Rice land	0.7633	0.9138	0.8062	0.7619	0.8953	0.8315	3.262×10^{-4}
S2	Dry land	0.7720	0.8920	0.8062	0.6667	1.0000	0.8523	4.126×10^{-4}
S3	Rice land	0.9966	0.9957	0.9964	0.3452	0.4823	0.6638	1.365×10^{-4}
S3	Dry land	0.9952	0.9940	0.9948	0.3452	0.4780	0.6615	2.021×10^{-4}

3.3.3. Evaluation and Optimum Selection of Eco-Compensation Scenarios

By comparing the results of E10 (Table 6), the "S2 on dry land" can be regarded as the best eco-compensation measure in MLW, followed by the "S2 on rice land". If only one of the above two measures is chosen, with the consideration of irregular distribution of the rice land and dry land within the watershed, the management difficulty and implementation cost will increase. Therefore, we think that the fallow scenario (S2) both on rice land and dry land is the best eco-compensation scenario in MLW for NPS pollution control.

It is also worth noting that the environmental effects (C6) of S3 are relatively optimal, but its C8 and D9 are lower due to its relatively lower compensation *COST* standard of current policy. If the compensation *COST* standard of S3 can be improved or phased compensation (higher compensation standard before the trees become timber and then lower) can be implemented in future, S3 can be further compared with S2.

4. Discussion

4.1. Qualitative Evaluation of Simulation Inaccuracy under Eco-Compensation Scenarios

After the calibration of the SWAT model, the performance of this SWAT model in the MLW is qualified for runoff simulation and TOT_N and TOT_P simulation but not as good as other similar studies that simulate hydrological processes by the SWAT model [21,22,46]. This may be caused by the applicability of the SWAT model. The SWAT model is a distributed hydrological model and suitable for hydrological simulation of large and medium watersheds [19], but the MLW is a small watershed with an area of 387.63 km2. For small watershed simulation, the input data need to be extremely accurate. For the simulation of large and medium scale, human activities can be assimilated in hydrological simulation. However, in a small watershed, these factors of human activities can not be ignored. This may bring some uncertainty to the calibration. In addition, the measured data used for calibrating TOT_N and TOT_P parameters is monitored once per month, which may cause some uncertainty in calibration work. Moreover, the planting and fertilization schedule for rice, dry crops, and orchards within the watershed are generalized to the same period. Although they are obtained by field investigation, they are still not completely consistent with the actual situation. These uncertainties are associated with the objective limitation of the study subjects and methods.

Furthermore, for most hydrological models, equifinality exists among different parameters [75,76]. This means that there are many groups of parameters that could lead to good simulation results, but parameter settings vary in each compositional simulation [77]; this may lead to uncertainty for different scenario simulations. The scenarios set in

this research are based on three different measures that may have a positive effect on decreasing nutrient loss. However, the detail for each scenario is set subjectively. The simulation results under each scenario also yield some uncertainties. However, the qualitative analysis for nutrient responses under different scenarios is influenced less by these uncertainties [78]. When considering equifinality for different parameters, more appropriate methods for analyzing nutrient responses under different scenarios require further investigation.

For the simulation of S3, considering the long-term character of the implementation of eco-compensation measures and the difficulty in obtaining the data for the simulation of the long growth process of forest, the calculation of the response is based on the simulation results in scenario with mature forest, rather than the simulation across two scenarios. Therefore, the simulation results are based on the assumption that the measures have been successfully carried out. These may also bring some uncertainty in scenario simulation.

4.2. Advice on NPS Pollution Control within MLW

The results from scenarios analysis indicate that agricultural eco-compensation measures aimed at reducing the application of chemical fertilizers are effective for reducing NPS pollution in the MLW. However, farmland eco-compensation will bring some economic and social effects on local householders and community. So, it is necessary to combine environmental, social, and economic effects into the scenario evaluation of eco-compensation.

The result of the SMCE model on the 10 m × 10 m grid scale indicates that the comprehensive effect of eco-compensation in different regions of the watershed has significant spatial differences, as well as shown in Figures 12 and 13. Obviously, a higher value of comprehensive effect (E10) can be achieved by selectively compensating for those grids that have a relatively high comprehensive effect. In each compensation scenario, the economic effects (C7) or social effects (C8) of all grids with the same land use are of the same value, which is the mean value calculated by the results of the questionnaire survey. Therefore, the spatial difference of the comprehensive effect of the same land use mainly comes from the difference of environmental effect (C6). As a consequence, the spatial and differentiated compensation can be further carried out in line with the spatial difference of C6, and the optimal compensation area can be determined by combining different land use types. If equipped with appropriate technological and management measures, eco-compensation measures on the grid scale will obtain better comprehensive effect and cost-effectiveness, which is both the necessity and significance of controlling agricultural NPS pollution by eco-compensation on a precise spatial scale.

In general, a good fertilization plan should be able to fulfill the crop requirements with low fertilizer. In this case, the widespread implementation of "optimal fertilizer use" [79] is very likely to be the best NPS control measure. However, the extent of pollution reduction by the method of "optimal fertilizer use" is usually not very large and has an upper limit. This method is not particularly suitable because the research area in this article is a national natural protected area, which needs to greatly reduce pollution. However, for the areas without developed economic conditions or nature reserve, they are significantly different from the study area of this paper, so it is necessary to fully study the weights of environmental, economic, and social effects and then recalculate the comprehensive effect according to the framework of this paper to determine the optimal compensation measures.

5. Conclusions

Three agricultural activity adjustment scenarios were designed in this research: S1 (halving fertilization every year), S2 (fallow every other year), and S3 (returning agricultural land to forest). The SWAT model constructed in this paper could basically meet the

requirements of the simulation application of runoff and pollution in Maoli Lake Watershed. The following major conclusions can be drawn:

(1) The nutrients loss of the agricultural land reduced in all scenarios, and S2 had more of a reduction compared to S1 and S3. The implementation of each scenario will have an impact on the farmers' farmland income, and the impact on S2 and S3 is relatively large. As the result of different compensation cost standards, farmers' willingness to participate in different scenarios is different. Their willingness to participate in S2 is the highest, followed by S1, and that of S3 is the lowest.
(2) With the combined perspective of environment–economy–society effects, the rice land and dry land fallow every other year (S2) is the best eco-compensation scenario in MLW for NPS pollution control in the near future.
(3) The comprehensive effect of eco-compensation at grid scale has significant spatial difference. When an eco-compensation scheme is used to control NPS pollution, a better result can be obtained by accurate and differentiated compensation on the precise spatial scale.
(4) This study was carried out from the perspective of combining SWAT and an eco-compensation scheme, which could broaden the application fields of the SWAT to some extent and provide a scientific basis and experience for the comprehensive evaluation and spatial design of agricultural eco-compensation.
(5) For the areas without developed economic conditions or nature reserve, they are significantly different from the study area of this paper, so it is necessary to fully study the weights of environmental, economic, and social effects and then recalculate the comprehensive effect according to the framework of this paper to determine the optimal compensation measures. The widespread implementation of "optimal fertilizer use" in this case is very likely to be the best NPS control measure.

Author Contributions: All the authors made significant contributions to the work. G.L. supervised the study. Y.Z. collected data, developed analysis models, and drafted the paper. P.Y. was responsible for data analysis, parallel calculation, and results verification. All authors made a contribution to writing, revising, and proofreading the manuscript. All authors have read and agreed to the published version of the manuscript.

Funding: This research was funded by the National Key Research and Development Program of China (Grant Number 2017YFC0405303), the Foundation of Humanity and Social Science of China Ministry of Education (Grant Number 20YJC630231), the Scientific Research Project of Education Department of Hunan Province of China (Grant Number 18K059), and the Science and Technology Research and Development Program of China State Construction Engineering Corporation Ltd. (Grant Number CSCEC-2021-Z-26 and CSCEC-2020-Z-43).

Institutional Review Board Statement: Not applicable.

Informed Consent Statement: Informed consent was obtained from all stakeholders involved in the study.

Data Availability Statement: The data are contained within this article and references.

Acknowledgments: The authors would like to thank Ting Liu (Management School, Swan College of Central South University of Forestry and Technology, China) for many helpful discussions and computer programming regarding research process and manuscript preparation.

Conflicts of Interest: The funders had no role in the design of the study; in the collection, analyses, or interpretation of data; in the writing of the manuscript, or in the decision to publish the results.

Appendix A

Table A1. Ranges and calibrated values of the sensitive parameters selected in this SWAT model.

Parameters[1]	Description	Initial Value	Range	Adjusted Value
R__CN2.mgt	SCS runoff curve number	67	(−0.5, 0.5)	0.12
V__SURLAG.bsn	Surface runoff lag time		(1, 24)	3.59
R__SOL_K.sol	Saturated hydraulic conductivity (mm/hr)	264.6	(−0.5, 0.5)	0.08
R__SOL_AWC.sol	Available water capacity of the soil layer (mm/mm)	0.344	(−0.5, 0.5)	−0.03
V__CANMX.hru	Maximum canopy storage		(0, 30)	4.29
V__GW_REVAP.gw	Groundwater "revap" coefficient		(0.02, 0.2)	0.09
V__REVAPMN.gw	Threshold depth of water in the shallow aquifer for "revap" to occur (mm)		(0, 1000)	49.92
V__GW_DELAY.gw	Groundwater delay (days)		(0, 500)	173.12
V__ALPHA_BF.gw	Baseflow alpha factor (days)		(0, 1)	0.39
V__GWQMN.gw	Threshold depth of water in the shallow aquifer required for return flow to occur (mm)		(0, 500)	91.32
V__ESCO.hru	Soil evaporation compensation factor		(0, 1)	0.19
V__EPCO.hru	Plant uptake compensation factor		(0, 1)	0.35
V__SPCON.bsn	Linear parameter for calculating the maximum amount of sediment that can be re-entrained during channel sediment routing		(0.001, 0.01)	0.015
V__SPEXP.bsn	Exponent parameter for calculating sediment reentrained in channel sediment routing		(1, 1.5)	1.38
R__USLE_P.mgt	USLE equation support practice factor	0.53	(−0.5, 0.5)	−0.35
V__CH_N2.rte	Manning's "n" value for the main channel		(0, 0.3)	0.11
V__SOL_ORGN.chm	Initial organic N concentration in the soil layer, (mg/kg).		(0, 100)	72.2
V__PHOSKD.bsn	Phosphorus soil partitioning coefficient.		(100, 200)	125
V__NPERCO.bsn	Nitrogen percolation coefficient		(0, 1)	0.35
V__SOL_ORGP.chm	Initial organic P concentration in surface soil layer, (mg/kg)		(0, 100)	85.9
V__CDN.bsn	Denitrification exponential rate coefficient		(0, 3)	0.72
V__PSP.bsn	Phosphorus sorption coefficient		(0.01, 0.7)	0.41
V__RCN.bsn	Concentration of nitrogen in rainfall		(0, 15)	2.3

[1] R__ means the existing parameter value is multiplied by (1 + an given value); V__ means the existing parameter value is to be replaced by the given value.

Appendix B

Table A2. Planting and fertilization management of each scenario in SWAT operations. S0: current situation; S1: halving fertilization every year; S2: fallow every other year; S3: returning agricultural land to forest.

Farmland Type	Measure	Measure Time	Land Cover	Fertilization management of each scenario kg/(ha·yr^{-1})				
				S0	S1	S2[(c)]	S2[(d)]	S3
Dry land	Sowing	1 Jan.				-		
	Fertilization	15 Mar.	Dry land	149.99[(b)]	74.99[(b)]	0	149.99[(b)]	149.99[(b)]
	Fertilization	15 Apr.	Dry land	112.49[(b)]	56.24[(b)]	0	112.49[(b)]	112.49[(b)]
	harvest and removing	15 May				-		
	Sowing	20 May				-		
	Fertilization	25 May	Dry land	899.96[(a)]	449.98[(a)]	0	899.96[(a)]	899.96[(a)]
	Fertilization	15 Jun.	Dry land	262.49[(b)]	131.24[(b)]	0	262.49[(b)]	262.49[(b)]
	Fertilization	15 Jul.	Dry land	224.89[(b)]	112.44[(b)]	0	224.89[(b)]	224.89[(b)]
	Fertilization	15 Aug.	Dry land	187.49[(b)]	93.74[(b)]	0	187.49[(b)]	187.49[(b)]

	harvest and removing	20 Oct.				-		
	Sowing	25 Oct.				-		
	Fertilization	30 Oct.	Dry land	674.97[(a)]	337.48[(a)]	0	674.97[(a)]	674.97[(a)]
	Fertilization	15 Nov.	Dry land	187.49[(b)]	93.745[(b)]	0	187.49[(b)]	187.49[(b)]
	harvest and removing	25 Dec.	Dry land			-		
Rice land	Sowing	1 Jan.				-		
	Fertilization	5 Jan.	Dry land	149.99[(b)]	74.99[(b)]	0	149.99[(b)]	149.99[(b)]
	Fertilization	10 Mar.	Dry land	112.49[(b)]	56.24[(b)]	0	112.49[(b)]	112.49[(b)]
	harvest and removing	20 Apr.				-		
	Sowing	25 Apr.				-		
	Fertilization	30 Apr.	Rice land	749.63[(a)]	374.81[(a)]	0	749.63[(a)]	749.63[(a)]
	Fertilization	15 May	Rice land	149.93[(b)]	74.96[(b)]	0	149.93[(b)]	149.93[(b)]
	Fertilization	15 Jul.	Rice land	149.93[(b)]	74.96[(b)]	0	149.93[(b)]	149.93[(b)]
	harvest and removing	25 Sep.				-		
	Sowing	1 Oct.				-		
	Fertilization	5 Oct.	Dry land	674.97[(a)]	337.48[(a)]	0	674.97[(a)]	674.97[(a)]
	Fertilization	10 Dec.	Dry land	187.49[(b)]	93.74[(b)]	0	187.49[(b)]	187.49[(b)]
	harvest and removing	25 Nov.				-		
Orchard	Fertilization	15 Mar.	Orchard	149.92[(a)]	74.96[(a)]	149.92[(a)]	149.92[(a)]	149.92[(a)]
	Fertilization	15 May	Orchard	374.81[(b)]	187.40[(b)]	374.81[(b)]	374.81[(b)]	374.81[(b)]
	harvest	15 Nov.						
	Fertilization	25 Nov.	Orchard	899.55[(b)]	449.77[(b)]	899.55[(b)]	899.55[(b)]	899.55[(b)]
Forest	-	-	Forest	0	0	0	0	0
Grass land	-	-	Pasture	0	0	0	0	0

[(a)]: Synthetic fertilizer; [(b)]: Urea; [(c)]: Fallow year of S2; [(d)]: Farming year of S2.

Appendix C

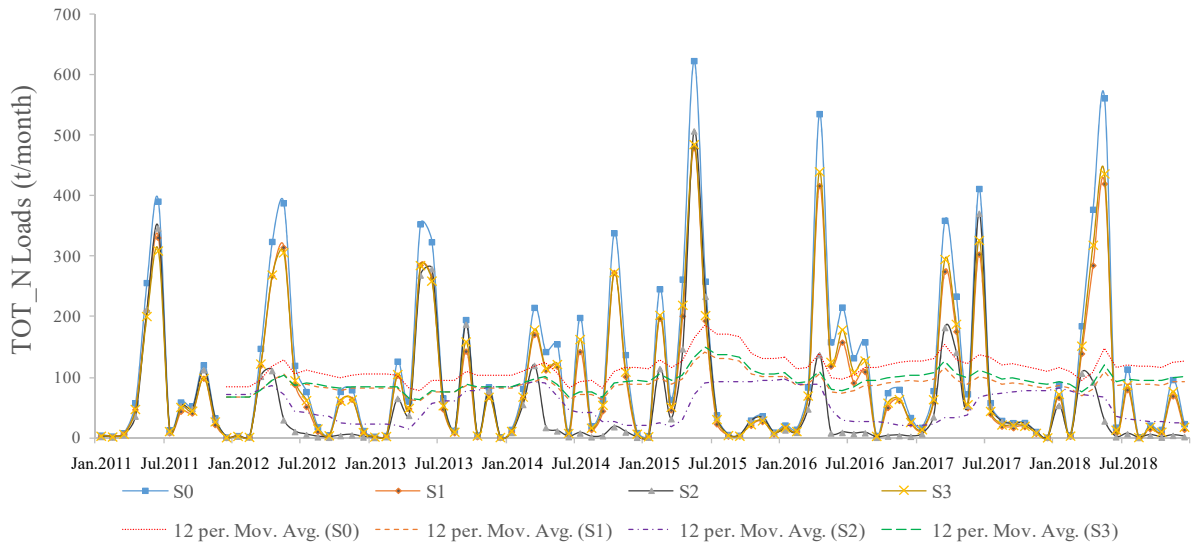

Figure A1. Simulation of monthly TOT_N load in MLW under different scenarios.

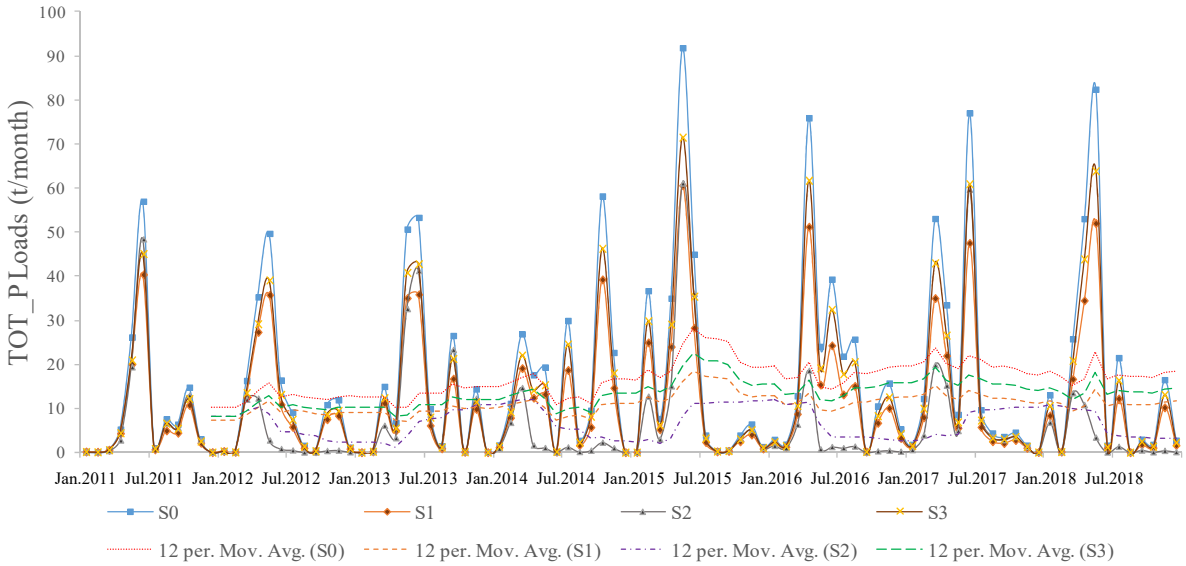

Figure A2. Simulation of monthly TOT_P load in MLW under different scenarios.

References

1. Cherry, K.; Shepherd, M.; Withers, P.; Mooney, S. Assessing the effectiveness of actions to mitigate nutrient loss from agriculture: A review of methods. *Sci. Total Environ.* **2008**, *406*, 1–23, doi:10.1016/j.scitotenv.2008.07.015.
2. Smith, L.E.; Siciliano, G. A comprehensive review of constraints to improved management of fertilizers in China and mitigation of diffuse water pollution from agriculture. *Agric. Ecosyst. Environ.* **2015**, *209*, 15–25, doi:10.1016/j.agee.2015.02.016.
3. Xueman, Y.; Wenxi, L.; Yongkai, A.; Dong, W. Assessment of parameter uncertainty for non-point source pollution mechanism modeling: A Bayesian-based approach. *Environ. Pollut.* **2020**, *263*, 114570, doi:10.1016/j.envpol.2020.114570.
4. Lu, H.; Xie, H. Impact of changes in labor resources and transfers of land use rights on agricultural non-point source pollution in Jiangsu Province, China. *J. Environ. Manag.* **2018**, *207*, 134–140, doi:10.1016/j.jenvman.2017.11.033.
5. Liu, G.; Wu, W.; Zhang, J. Regional differentiation of non-point source pollution of agriculture-derived nitrate nitrogen in groundwater in northern China. *Agric. Ecosyst. Environ.* **2005**, *107*, 211–220, doi:10.1016/j.agee.2004.11.010.
6. Haregeweyn, N.; Yohannes, F. Testing and evaluation of the agricultural non-point source pollution model (AGNPS) on Augucho catchment, western Hararghe, Ethiopia. *Agric. Ecosyst. Environ.* **2003**, *99*, 201–212, doi:10.1016/S0167-8809(02)00120-2.
7. Lai, Y.; Yang, C.; Hsieh, C.; Wu, C.; Kao, C. Evaluation of non-point source pollution and river water quality using a multimedia two-model system. *J. Hydrol.* **2011**, *409*, 583–595, doi:10.1016/j.jhydrol.2011.08.040.
8. Zhang, P.; Liu, Y.; Pan, Y.; Yu, Z. Land use pattern optimization based on CLUE-S and SWAT models for agricultural non-point source pollution control. *Math. Comput. Model.* **2013**, *58*, 588–595, doi:10.1016/j.mcm.2011.10.061.
9. Xiang, C.; Wang, Y.; Liu, H. A scientometrics review on nonpoint source pollution research. *Ecol. Eng.* **2017**, *99*, 400–408, doi:10.1016/j.ecoleng.2016.11.028.
10. Chowdary, V.; Kar, S.; Adiga, S. Modelling of non-point source pollution in a watershed using remote sensing and GIS. *J. Indian Soc. Remote Sens.* **2004**, *32*, 59–73, doi:10.1007/BF03030848.
11. Kinnell, P. AGNPS-UM: Applying the USLE-M within the agricultural non point source pollution model. *Environ. Model. Softw.* **2000**, *15*, 331–341, doi:10.1016/S1364-8152(00)00002-5.
12. Wu, L.; Gao, J.; Ma, X.; Li, D. Application of modified export coefficient method on the load estimation of non-point source nitrogen and phosphorus pollution of soil and water loss in semiarid regions. *Environ. Sci. Pollut. Res.* **2015**, *22*, 10647–10660, doi:10.1007/s11356-015-4242-z.
13. Borah, D.K.; Bera, M. Watershed-scale hydrologic and nonpoint-source pollution models: Review of applications. *Trans. ASAE* **2004**, *47*, 789, doi:10.13031/2013.16110.
14. Adu, J.T.; Kumarasamy, M.V. Assessing Non-Point Source Pollution Models: A Review. *Pol. J. Environ. Stud.* **2018**, 27, doi:10.15244/pjoes/76497.
15. Gikas, G.D.; Yiannakopoulou, T.; Tsihrintzis, V.A. Modeling of non-point source pollution in a Mediterranean drainage basin. *Environ. Modeling Assess.* **2006**, *11*, 219–233, doi:10.1007/s10666-005-9017-3.
16. Polyakov, V.; Fares, A.; Kubo, D.; Jacobi, J.; Smith, C. Evaluation of a non-point source pollution model, AnnAGNPS, in a tropical watershed. *Environ. Model. Softw.* **2007**, *22*, 1617–1627, doi:10.1016/j.envsoft.2006.12.001.
17. Wang, H.; Wu, Z.; Hu, C. A comprehensive study of the effect of input data on hydrology and non-point source pollution modeling. *Water Resour. Manag.* **2015**, *29*, 1505–1521, doi:10.1007/s11269-014-0890-x.
18. Cao, D.; Cao, W.; Fang, J.; Cai, L. Nitrogen and phosphorus losses from agricultural systems in China: A meta-analysis. *Mar. Pollut. Bull.* **2014**, *85*, 727–732, doi:10.1016/j.marpolbul.2014.05.041.
19. Arnold, J.G.; Williams, J.R.; Maidment, D.R. Continuous-time water and sediment-routing model for large basins. *J. Hydraul.*

Eng. **1995**, *121*, 171–183, doi:10.1061/(ASCE)0733-9429(1995)121:2(171).
20. Yang, S.; Dong, G.; Zheng, D.; Xiao, H.; Gao, Y.; Lang, Y. Coupling Xinanjiang model and SWAT to simulate agricultural non-point source pollution in Songtao watershed of Hainan, China. *Ecol. Model.* **2011**, *222*, 3701–3717, doi:10.1016/j.ecolmodel.2011.09.004.
21. Wang, Q.; Liu, R.; Men, C.; Guo, L. Application of genetic algorithm to land use optimization for non-point source pollution control based on CLUE-S and SWAT. *J. Hydrol.* **2018**, *560*, 86–96, doi:10.1016/j.jhydrol.2018.03.022.
22. Abbaspour, K.C.; Rouholahnejad, E.; Vaghefi, S.; Srinivasan, R. A continental-scale hydrology and water quality model for Europe: Calibration and uncertainty of a high-resolution large-scale SWAT model. *J. Hydrol.* **2015**, *524*, 733–752, doi:10.1016/j.jhydrol.2015.03.027.
23. Geng, R.; Sharpley, A.N. A novel spatial optimization model for achieve the trad-offs placement of best management practices for agricultural non-point source pollution control at multi-spatial scales. *J. Clean. Prod.* **2019**, *234*, 1023–1032, doi:10.1016/j.jclepro.2019.06.277.
24. Sharpley, A.N.; Kleinman, P.J.; Flaten, D.N.; Buda, A.R. Critical source area management of agricultural phosphorus: Experiences, challenges and opportunities. *Water Sci. Technol.* **2011**, *64*, 945–952, doi:10.2166/wst.2011.712.
25. Maringanti, C.; Chaubey, I.; Popp, J. Development of a multiobjective optimization tool for the selection and placement of best management practices for nonpoint source pollution control. *Water Resour. Res.* **2009**, *45*, doi:10.1029/2008WR007094.
26. Zhong, H.; Qing, P.; Hu, W. Farmers' willingness to participate in best management practices in Kentucky. *J. Environ. Plan. Manag.* **2016**, *59*, 1015–1039, doi:10.1080/09640568.2015.1052379.
27. Link, J.; Graeff, S.; Batchelor, W.D.; Claupein, W. Evaluating the economic and environmental impact of environmental compensation payment policy under uniform and variable-rate nitrogen management. *Agric. Syst.* **2006**, *91*, 135–153, doi:10.1016/j.agsy.2006.02.003.
28. The Research Group on Mechanism and Policy of Eco-compensation in China. *The Research on Mechanism and Policy of Eco-compensation in China*; Science Press: Beijing, China, 2007. (In Chinese)
29. Wunder, S. Payments for Environmental Services: Some Nuts and Bolts. 2005. Available online: http://hdl.handle.net/10919/66932 (accessed on 1 January 2005).
30. Wunder, S. When payments for environmental services will work for conservation. *Conserv. Lett.* **2013**, *6*, 230–237, doi:10.1111/conl.12034.
31. Firbank, L.; Bradbury, R.B.; McCracken, D.I.; Stoate, C. Delivering multiple ecosystem services from Enclosed Farmland in the UK. *Agric. Ecosyst. Environ.* **2013**, *166*, 65–75, doi:10.1016/j.agee.2011.11.014.
32. Cong, R.G.; Smith, H.G.; Olsson, O.; Brady, M. Managing ecosystem services for agriculture: Will landscape-scale management pay?. *Ecol. Econ.* **2014**, *99*, 53–62, doi:10.1016/j.ecolecon.2014.01.007.
33. Jack, B.K.; Kousky, C.; Sims, K.R. Designing payments for ecosystem services: Lessons from previous experience with incentive-based mechanisms. *Proc. Natl. Acad. Sci. USA* **2008**, *105*, 9465–9470, doi:10.1073/pnas.0705503104.
34. Kerr, S.; Greenhalgh, S.; Simmons, G. The Taupo Nitrogen Market: The World's Only Diffuse Source Trading Programme. MOTU Note #20. Motu Public Policy and Research, Wellington. 2015. Available online: http://www.motu.org.nz/assets/Documents/our-work/environment-and resources/nutrient-trading-and-water-quality/Motu-Note-20-Taupo-Nitrogen-Market (accessed on 16 January 2015).
35. Aguilar, F.X.; Obeng, E.A.; Cai, Z. Water quality improvements elicit consistent willingness-to-pay for the enhancement of forested watershed ecosystem services. *Ecosyst. Serv.* **2018**, *30*, 158–171, doi:10.1016/j.ecoser.2018.02.012.
36. McGurk, E.; Hynes, S.; Thorne, F. Participation in agri-environmental schemes: A contingent valuation study of farmers in Ireland. *J. Environ. Manag.* **2020**, *262*, 110243, doi:10.1016/j.jenvman.2020.110243.
37. Ma, S.; Swinton, S.M.; Lupi, F.; Jolejole-Foreman, C. Farmers' willingness to participate in Payment-for-Environmental-Services programmes. *J. Agric. Econ.* **2012**, *63*, 604–626, doi:10.1111/j.1477-9552.2012.00358.x.
38. Beharry-Borg, N.; Smart, J.C.; Termansen, M.; Hubacek, K. Evaluating farmers' likely participation in a payment programme for water quality protection in the UK uplands. *Reg. Environ. Chang.* **2013**, *13*, 633–647, doi:10.1007/s10113-012-0282-9.
39. Talberth, J.; Selman, M.; Walker, S.; Gray, E. Pay for Performance: Optimizing public investments in agricultural best management practices in the Chesapeake Bay Watershed. *Ecol. Econ.* **2015**, *118*, 252–261, doi:10.1016/j.ecolecon.2015.07.033.
40. Saarikoski, H.; Mustajoki, J.; Barton, D.N.; Geneletti, D. Multi-Criteria Decision Analysis and Cost-Benefit Analysis: Comparing alternative frameworks for integrated valuation of ecosystem services. *Ecosyst. Serv.* **2016**, *22*, 238–249, doi:10.1016/j.ecoser.2016.10.014.
41. Tian, F.; Yi, H.; Fu, B.; Yang, Y.; Qiu, G.; Zhang, L. Effects of ecological engineering on water balance under two different vegetation scenarios in the Qilian Mountain, northwestern China. *J. Hydrol. Reg. Stud.* **2015**, doi:10.1016/j.ejrh.2015.11.015.
42. Basheer, A.K.; Lu, H.; Omer, A.; Ali, A.; Abdelgader, A. Impacts of climate change under CMIP5 RCP scenarios on the streamflow in the Dinder River and ecosystem habitats in Dinder National Park, Sudan. *Hydrol. Earth Syst. Sci.* **2016**, *20*, 1331–1353, doi:10.5194/hess-20-1331-2016.
43. Hu, J.Y.; Wu, Y.; Wang, L.; Sun, P.; Lian, Y. Impacts of land-use conversions on the water cycle in a typical watershed in the southern Chinese Loess Plateau. *J. Hydrol.* **2021**, *593*, 125741, doi:10.1016/j.jhydrol.2020.125741.
44. Cao, X. Maoli Lake: A Transformation from Turbid to Limpidly. Hunan Daily. Available online: https://hnrb.voc.com.cn/hnrb_epaper/html/2015-10/20/content_1023619.htm?div=-1 (accessed on 20 October 2015).
45. Alibuyog, N.R.; Ella, V.B.; Reyes, M.R.; Srinivasan, R; Dillaha, T. Predicting the effects of land use change on runoff and sediment

yield in Manupali River subwatersheds using the SWAT model. *Int. Agric. Eng. J.* **2009**, *18*, 15–25.
46. Xu, Z.X.; Pang, J.P.; Liu, C.M.; Li, J. Assessment of runoff and sediment yield in the Miyun Reservoir catchment by using SWAT model. *Hydrol. Process.* **2009**, *23*, 3619–3630, doi:10.1002/hyp.7475.
47. Lin, Z.; Radcliffe, D.E.; Risse, L.M.; Romeis, J.J.; Jackson, C.R. Modeling phosphorus in the Lake Allatoona watershed using SWAT: II. Effect of land use change. *J. Environ. Qual.* **2009**, *38*, 121–129, doi:10.2134/jeq2007.0111.
48. Neitsch, S.L.; Arnold, J.G.; Kiniry, J.R.; Williams, J.R. Soil and water assessment tool theoretical documentation. *Comput. Speech Lang.* **2011**, *24*, 289–306, doi:10.1016/j.csl.2009.04.006.
49. Williams, J.R. Chapter 25. The EPIC Model. In *Computer Models of Watershed Hydrology*; Water Resources Publications: Highlands Ranch, CO, USA, 1995; pp. 909–1000.
50. McElroy, A.D.; Chiu, S.Y.; Nebgen, J.W.; Aleti, A.; Bennett, F.W. 1976. *Loading Functions for Assessment of Water Pollution from Nonpoint Sources*; EPA 600/2-76-151; US Environmental Protection Agency, Office of Research and Development: Washington DC, USA, 1976.
51. Williams, J.R.; Hann, R.W. *Optimal Operation of Large Agricultural Watersheds with Water Quality Constraints*; Texas A&M Univ., Tech. Rept. No. 96; Texas Water Resources Institute: Dallas, TX, USA 1978.
52. Long, Y.; Tang, R.; Wang, H.; Jiang, C. Monthly precipitation modeling using Bayesian non-homogeneous hidden Markov Chain. *Hydrology Research*. **2019**, 50, 562-576, doi:10.2166/nh.2018.077.
53. Abbaspour, K.C. *SWAT-Cup 2012: SWAT Calibration and Uncertainty Programs—A User Manual*; Eawag, Swiss Federal Institute of Aquatic Science and Technology: Duebendorf, Switzerland, 2014.
54. Abbaspour, K.C.; Vaghefi, S.A.; Srinivasan, R. A Guideline for Successful Calibration and Uncertainty Analysis for Soil and Water Assessment: A Review of Papers from the 2016 International SWAT Conference. *Water* **2017**, *10*, 6, doi:10.3390/w10010006.
55. Abbaspour, K.C.; Jing, Y.; Maximov, I.; Siber, R.; Srinivasan, R. Modelling of Hydrology and Water Quality in the Pre-Alpine/Alpine Thur Watershed Using SWAT. *J. Hydrol.* **2007**, *333*, 413–430, doi:10.1016/j.jhydrol.2006.09.014.
56. Niraula, R.; Norman, L.M.; Meixner, T.; Callegary, J.B. Multi-gauge Calibration for modeling the Semi-Arid Santa Cruz Watershed in Arizona-Mexico Border Area Using SWAT. *Air Soil Water Res.* **2012**, *5*, 41–57, doi:10.4137/ASWR.S9410.
57. Li, D.; Liang, X.; Wu, J. Water pollution risk simulation and prediction in a drinking water catchment. *J. Zhejiang Univ.* (*Agric. Life Sci.*) **2018**, *44*, 75–88, doi:10.3785/j.issn.1008-9209.2017.05.222.
58. Moriasi, D.N.; Gitau, M.W.; Pai, N.; Daggupati, P. Hydrologic and water quality models: Performance measures and evaluation criteria. *Trans. Asabe* **2015**, *58*, 1763–1785, doi:10.13031/trans.58.10715.
59. Mamo, K.H.M.; Jain, M.K. Runoff and sediment modeling using SWAT in Gumera catchment, Ethiopia. *Open J. Mod. Hydrol.* **2013**, *2013*, doi:10.4236/ojmh.2013.34024.
60. Rahbeh, M.; Chanasyk, D.; Miller, J. Two-way calibration-validation of SWAT model for a small prairie watershed with short observed record. *Can. Water Resour. J. Rev. Can. Des Ressour. Hydr.* **2011**, *36*, 247–270, doi:10.4296/cwrj3603884.
61. Chuanzhun, S.; Lin, Z.; Chao, W. Biodiversity simulation of Poyang Lake wetlands by InVEST model under different scenarios. *Resour. Environ. Yangtze Basin* **2015**, *24*, 1119–1125.
62. Xie, H.; Cheng, L.; Lv, T. Factors influencing farmer willingness to fallow winter wheat and ecological compensation standards in a groundwater funnel area in Hengshui, Hebei Province, China. *Sustainability* **2017**, *9*, 839, doi:10.3390/su9050839.
63. Liu, J.; Li, S.; Ouyang, Z.; Tam, C.; Chen, X. Ecological and socioeconomic effects of China's policies for ecosystem services. *Proc. Natl. Acad. Sci.* **2008**, *105*, 9477–9482, doi:10.1073/pnas.0706436105.
64. Wu, Y.; Liu, J.; Shen, R.; Fu, B. Mitigation of nonpoint source pollution in rural areas: From control to synergies of multi ecosystem services. *Sci. Total Environ.* **2017**, *607*, 1376–1380, doi:10.1016/j.scitotenv.2017.07.105.
65. Omid, G.; Bakhtiar, F.; Thomas, B. An interval matrix method used to optimize the decision matrix in AHP technique for land subsidence susceptibility mapping. *Environ. Earth Ences* **2018**, *77*, 584, doi:10.1007/s12665-018-7758-y.
66. Bennett, D.E.; Gosnell, H. Integrating multiple perspectives on payments for ecosystem services through a social–ecological systems framework. *Ecol. Econ.* **2015**, *116*, 172–181, doi:10.1016/j.ecolecon.2015.04.019.
67. Huber, R.; Briner, S.; Peringer, A.; Lauber, S.; Seidl, R.; Widmer, A.; Gillet, F.; Buttler, A.; Le, Q.B.; Hirschi, C. 2013. Modeling social-ecological feedback effects in the implementation of payments for environmental services in pasture-woodlands. *Ecol. Soc.* **2013**, *18*, 41, doi:10.5751/ES-05487-180241.
68. Moore, R.; Provencher, B.; Bishop, R. Valuing a Spatially Variable Environmental Resource:Reducing Non-Point-Source Pollution in Green Bay, Wisconsin. *Land Econ.* **2011**, doi:10.3368/le.87.1.45.
69. Cao, S.; Xia, C.; Xian, J.; Guo, H.; Zheng, H. Payoff of the Grain for Green policy. *J. Appl. Ecol.* **2020**, *57*, doi:10.1111/1365-2664.13608.
70. Yuan, P.; Li, D.J.; Cai, C.S.; Xu, G.J. A novel decoupling dynamic method with third-order accuracy and controllable dissipation. *Computers & Structures.* **2021**, 249, 44-56, doi:10.1016/j.compstruc.2021.106512.
71. LI, G.; SHI, H. The Payment of Grain to Green Project, the Behavior Choice of Peasants and Their Gains and Losses. *China Popul. Resour. Environ.* **2015**, *25*, 152–161, doi:10.3969/j.issn.1002-2104.2015.05.020.
72. Liu, D.; Hu, Z.; Jin, L. Study on compensation rate for fallow program in groundwater over-exploited area based on rural households' willingness to accept. *China Popul. Resour. Env.* **2019**, *29*, 130–139.
73. Gonzalezredin, J.; Luque, S.; Poggio, L.; Smith, R.; Gimona, A. Spatial Bayesian belief networks as a planning decision tool for mapping ecosystem services trade-offs on forested landscapes. *Environ. Res.* **2016**, 144, 15–26, doi:10.1016/j.envres.2015.11.009.
74. Liu, J.W.; Li, D.J.; Yu, P. Study on optimization algorithm of tuned mass damper parameters to reduce vehicle-bridge coupled

vibration. *PLoS ONE.* **2019**, *14*, e0215773, doi:10.1371/journal.pone.0215773.
75. Khatami, S.; Peel, M.C.; Peterson, T.J.; Western, A. Equifinality and flux mapping: A new approach to model evaluation and process representation under uncertainty. *Water Resour. Res.* **2019**, *55*, 8922–8941, doi:10.1029/2018WR023750.
76. Yuan, P.; Li, D.J.; Cai, C.S.; Xu, G.J. An efficient decoupling dynamic algorithm for coupled multi-spring-systems. *Computers & Structures.* **2018**, *209*, 44-56, doi:10.1016/j.compstruc.2018.08.012.
77. Teweldebrhan, A.T.; Burkhart, J.F.; Schuler, T.V. Parameter uncertainty analysis for an operational hydrological model using residual-based and limits of acceptability approaches. *Hydrol. Earth Syst. Sci.* **2018**, *22*, 5021–5039, doi:10.5194/hess-2018-158.
78. Moges, E.; Demissie, Y.; Larsen, L.; Yassin, F. Sources of Hydrological Model Uncertainties and Advances in Their Analysis. *Water* **2020**, *13*, 28, doi:10.3390/w13010028.
79. Che, S.G.; Zhao, B.Q.; Ting, L.Y.; Yuan, L.; Lin, Z.; Wen, H.; Shen, B. Nutrient uptake requirements with increasing grain yield for rice in China. *J. Integr. Agric.* **2016**, *15*, 907–917, doi:10.1016/S2095-3119(15)61143-1.